WIDE BANDGAP SEMICONDUCTOR DESIGN, PROCESSING, AND CHARACTERIZATION

By

JIHYUN KIM

A DISSERTATION PRESENTED TO THE GRADUATE SCHOOL
OF THE UNIVERSITY OF FLORIDA IN PARTIAL FULFILLMENT
OF THE REQUIREMENTS FOR THE DEGREE OF
DOCTOR OF PHILOSOPHY

UNIVERSITY OF FLORIDA

2004

Copyright 2004

by

Jihyun Kim

To my family

ACKNOWLEDGMENTS

Many people have assisted me and offered their support. I would like to express my appreciation to them.

Professor Fan Ren has been guiding me to the right way. I am indebted to him a lot. Also I appreciate Professor Stephen J. Pearton and Professor Cammy R. Abernathy for their fruitful advices and kindness.

Also, I really thank Dr. Brent Gila for growing good samples for me. Most of the samples were from him, and his Rusty. And I was happy to meet Dr. Gilyong Chung because of his help and his SiC samples. I had a great time in Murray Hill, NJ with Dr. Hock Min Ng at Bell Labs as an intern. I appreciate his having me there. And I thank Dr. Yun Daniel Park for giving me advice and his help with magnetic materials.

I owe our research group members a lot of things. I will never forget the days working with them in the cleanroom. I thank Drs. Wayne Johnson, Anping Zhang, Gerard Dang, Jeff LaRoche, Suku Kim, Wen-Ben Luo, Kyu-pil Lee, Mark Overberg and Irokawa Yoshihiro and hope Kimberly, Andrea, Rachel, Jerry, Rishabh, Byong Sam, Soohwan, Kelly, and Kwang can complete their research well. Also, I wish to thank Jang Y. Hwang and other Korean graduate students for kind advices.

Finally, for the support from my family, Jiwan, Jibum, my parents, and my grand parents, I really thank them. And I thank and love my wife, Heejo for her support.

TABLE OF CONTENTS

page

ACKNOWLEDGMENTS iv

LIST OF TABLES viii

LIST OF FIGURES ix

ABSTRACT xii

1 INTRODUCTION 1

1.1 Motivation 1
1.2 Dissertation Outline 2

2 LITERATURE REVIEW AND BACKGROUND 9

2.1 Historical Review 9
2.2 Background 11
2.2.1 Traps in device 11
2.2.1.1 Mobile ions 11
2.2.1.2 Fixed oxide charge 12
2.2.1.3 Interface trap 12
2.2.2 Interface trap density measurement techniques 13
2.2.2.1 High-low frequency capacitance-voltage method 13
2.2.2.2. Low frequency capacitance method 14
2.2.2.3. High frequency capacitance method 14
2.2.2.4. AC conductance method 16

3 GALLIUM NITRIDE BASED METAL-OXIDE-SEMICONDUCTOR DIODES 22

3.1 Introduction 22
3.2 Molecular Beam Epitaxy Oxide Growth 24
3.2.1 Growth of MgO on GaN 24
3.2.2 Growth of Sc_2O_3 on GaN 25

3.3 GaN Based MOS Diode Fabrication 25
3.3.1 MgO/n-GaN MOS Diode Fabrication 25
3.3.2 MgO/p-GaN Gate-Controlled Diodes Fabrication 25
3.3.3 Sc_2O_3/p-GaN Gate-Controlled Diodes Fabrication 26
3.4 Diode DC and AC Characteristics 27
3.4.1 MgO/n-GaN MOS Diodes 27
3.4.2 MgO/GaN Gate-Controlled MOS Diodes 29
3.4.3 Sc_2O_3/GaN Gate-Controlled Diodes 30

4 SCHOTTKY METALLIZATION ON WIDE BANDGAP SEMICONDUCTORS FOR THE APPLICATIONS IN HARSH ENVIRONMENT 49

4.1. Introduction 49
4.2 Schottky Diode Processing 51
4.2.1 WSi_X/GaN Schottky Diode 51
4.2.2 WSi_X/SiC Schottky Diode 51
4.2.3 Gamma-Ray Irradiation to Schottky Diodes 52
4.3 Results and Discussion 52
4.3.1 WSi_X/GaN Schottky Diode 52
4.3.2 WSi_X/SiC Schottky Diode 54
4.3.3 Comparison of Stability of WSix/SiC and Ni/SiC Schottky Rectifiers to High Dose of Gamma-Ray Irradiation 57

5 WIDE BANDGAP GAS SENSORS 73

5.1 Introduction 73
5.2 Device Processing 74
5.2.1 4H-SiC Gas Sensors 74
5.2.2 GaN Gas Sensors 74
5.3 Characteristics of SiC and GaN Based Gas Sensors 75
5.3.1 Characteristics of Pt/4H-SiC Gas Sensors 75
5.3.2 Hydrogen-Sensitive GaN Schottky Diodes 76

6 SUMMARY AND FUTURE WORK 92

6.1 GaN MOS Diodes 92
6.2 MgO/GaN Gate-controlled Diodes 92
6.3 Inversion Behavior in Sc_2O_3/GaN Gate-controlled Diodes 93
6.4 Thermal Stability of WSi_X and W Metallization on GaN 94
6.5 Thermal Stability of WSi_X Schottky Contacts on 4H-SiC 94
6.6 High Dose Gamma-ray Irradiation on Rectifiers 95
6.7 Characteristics of SiC Gas Sensors 95
6.8 GaN Hydrogen Sensors 96

LIST OF REFERENCES 97

BIOGRAPHICAL SKETCH 106

LIST OF TABLES

Table page

Table 4-1 Barrier heights of WSi_X/GaN contacts as a function of anneal temperature.....59

Table 4-2 Summary of electrical data for annealed contacts.....60

Table 4-3 Summary of electrical data as a function of measurement temperature.....61

Table 4-4 Characteristics of SiC Rectifiers before and after Co-60 γ-ray irradiations.....62

LIST OF FIGURES

Figure page

Figure 1-1 Moor's Law for Intel CPU from 1971 to 2000 5

Figure 1-2 Intrinsic carrier concentration as a function of temperature for Si, GaAs, and GaN 6

Figure 1-3 Evolution of LEDs.[Pon97] 7

Figure 1-4 Energy bandgap diagram of compound and elemental semiconductors.....8

Figure 2-1 Calculated microwave device performance[Zha03a].....17

Figure 2-2 Traps in MOS structure[Pie96] 18

Figure 2-3 Interfacial Traps[Pie96] 19

Figure 2-4 Origin of interfacial traps in SiO_2[Pie96].....20

Figure 2-5 Passivation of interfacial traps[Pie96] 21

Figure 3-1 The overview of MBE system.....33

Figure 3-2 Cross-sectional view of a GaN diode with MgO as the gate oxide 34

Figure 3-3 TEM picture of MgO/GaN sample 35

Figure 3-4 Diode characteristics of a 100 nm thick MgO/GaN diode.....36

Figure 3-5 Typical C-V curve of a MgO/GaN diode under dark conditions at room temperature.....37

Figure 3-7 Schematic cross-section of n+p GaN MOS gate-controlled diode(top) and SEM plan view of device layout 39

Figure 3-8 Microscope View of device layout 40

Figure 3-9 1MHz C-V characteristic at 25°C of 40 μm diameter Pt/Au contact ,conventional MgO/p-GaN diode without any n^+ region to act a source of minority carriers.....41

Figure 3-10 C-V characteristics of GaN MOS gate-controlled diodes at 25°C as a function of measurement frequency(+15V bias in gated contact in each case). 42

Figure 3-12 Schematic of Sc_2O_3/p-GaN gate-controlled diodes.....44

Figure 3-13 Temperature dependence of 150 kHz C-V characteristics for ungated Sc_2O_3/p-GaN MIS diodes without source of minority carriers. 45

Figure 3-14 C-V characteristics of Sc_2O_3/p-GaN gated diodes as a function of drain bias at 25°C in the dark. The voltage ramp rate was 0.05 $V \cdot s^{-1}$ and measurement frequency 150kHz 46

Figure 3-15 C-V characteristics of Sc_2O_3/p-GaN gated diodes as a function of drain bias at 25°C in the dark. The voltage ramp rate was 0.1 $V \cdot s^{-1}$ and measurement frequency 200kHz 47

Figure 3-16 C-V characteristics of Sc_2O_3/p-GaN gated diodes as a function of measurement frequency at 25°C. The voltage ramp rate was 0.05 $V \cdot s^{-1}$ and there was zero drain bias 48

Figure 4-1 Schematic of WSiX/n-GaN Schottky diode.....63

Figure 4-2 Forward(top) and reverse(bottom) I-V characteristics from W/GaN diodes as a function of anneal temperature.....64

Figure 4-4 Schematic of WSi_X/SiC Schottky Diode.....66

Figure 4-5 Forward(top) and reverse(bottom) I-V characteristics from WSiX diodes on 4H-SiC as a function of post-depositon annealing temperature.....67

Figure 4-6 Forward I-V characteristics from Ni(top) and WSi_X(bottom) diodes on 4H-SiC as a function of measurement temperature. The WSi_X contacts were annealed at 500°C for 1min after deposition.....68

Figure 4-8 Schematic of SiC Schottky rectifiers. 70

Figure 4-9 Forward I-V characteristics of WSiX/SiC and Ni/SiC rectifiers before and after Co-60 γ-irradiation to doses up to 315Mrad 71

Figure 4-10 Optical micrographs of Ni(top) and WSiX/Ti/Au(bottom) contacts before and after Co-60 γ-irradiation to a dose of 315Mrad. The width of each micrograph is 40μm 72

Figure 5-1 Schematic of Pt/4H-SiC gas sensor.....80

Figure 5-2 High forward bias I-V characteristic from SiC sensor in pure N_2 or 10%H_2 in N_2 ambients at 25°C.(80μm diameter) 81

Figure 5-3 Log forward bias I-V characteristics from SiC sensor in 10%H2 in N2, pure N2 or CF4 ambients at 25°C. (80μm diameter). 82

Figure 5-4 Low bias forward I-V characteristics from SiC sensor in 10%H_2 in N_2 or pure N_2 ambients at the different temperatures.(Size of contact is 0.5cm×0.5cm). 83

Figure 5-6 Photograph of completed Pt/n-GaN diode 85

Figure 5-7 Time response at 110°C of forward current of a Pt/GaN diode forward biased at 1.5V, upon switching from N_2 ambient to 10% H_2 in N_2 and then back to N_2. ...86

Figure 5-8 Time response at 100°C of forward current of a Pt/GaN diode biased at 1.5V, upon cycling the ambient between pure N_2 and 10% H_2 in N_2. 87

Figure 5-9 Decay of forward current as a function of measuremental temperature for Pt/GaN diodes at 1.5V forward bias after switching from 10% H_2 in N_2 ambient to pure N_2.....88

Figure 5-10 Arrhenius plot of change in forward current of Pt/GaN diodes 50 secs after switching from 10% H_2 in N_2 ambient to pure N_2. 89

Figure 5-11 Forward I-V characteristics from Pd/GaN diodes measured in N_2 or 10% H_2 in N_2 ambient at either 170°C(top) or 200°C(bottom). 90

Figure 5-12 Forward current at 0.5V bias at 150°C(top) or 200°C(bottom) for Pd/GaN diodes cycled in N_2 and 10% H_2 in N_2 ambient. 91

Abstract of Dissertation Presented to the Graduate School
of the University of Florida in Partial Fulfillment of the
Requirements for the Degree of Doctor of Philosophy

WIDE BANDGAP SEMICONDUCTOR DESIGN, PROCESSING, AND CHARACTERIZATION

By

Jihyun Kim

MAY 2004

Chair: Fan Ren
Major Department: Chemical Engineering

Wide bandgap semiconductors have shown promising results in high power, high frequency, and high temperature application. There is also huge interest in the development of MOSFET due to lower power consumption, larger voltage swing, and better stability. Since the minority carrier generation rate of gallium nitride(GaN) is extremely slow, it is very difficult to achieve the inversion under the gate using conventional way. Unlike Silicon, GaN does not have high quality native oxide, instead novel oxides such as magnesium oxide(MgO) and scandium oxide(Sc_2O_3) were employed as the gate oxides for GaN based MOSFET. This dissertation contains the first demonstration of inversion using both MgO and Sc_2O_3 as the gate oxides. Gate-controlled diodes were successfully fabricated to supply minority carriers to under the gate region by implanting Si ions around gate area.

Most applications in wide bandgap semiconductors are required to be operated in a harsh environment, therefore, the degradation of metal contacts is critical for long term

stability of the devices. Tungsten(W) and tungsten silicide(WSi) based refractory metallizations were deposited on both GaN and SiC using sputter technique for the applications of high temperature operations. However, damage was introduced to the semiconductor due to ion bombardment during the sputtering and post-sputtering high temperature annealing is required to remove the ion bombardment damage. The optimum condition of the thermal annealing was found by measuring current-voltage to achieve low diode turn-on resistance and highest barrier height. A study of the effect for γ-irradiation on the stability of different metallizations was conducted. W and WSi based metallization contacts displayed superior stability as compared to nickel(Ni) contacts under irradiation condition.

Since wide bandgap semiconductors can stand high temperature, they can be fabricated into sensors that operate at elevated temperatures such as engines and reactors. Hydrogen sensors using both platinum(Pt) and palladium(Pd) as Schottky contacts have been demonstrated. With introduction of hydrogen gas to the GaN Schottky diodes, the barrier height of catalytic Schottky contacts was changed. The change of the Schottky barrier height was fully reversible.

CHAPTER 1
INTRODUCTION

1.1 Motivation

With the impressive development of the 'Information Age', the transistors have became the most numerous man-made object on our planet[Sah88]. After W. Shockley proposed and characterized the junction field effect transistor(J-FET) in 1952[Sch52], the metal-oxide-semiconductor(MOSFET) became the commercial products by RCA and Fairchild Semiconductor in 1960s. Since then the Si-based semiconductor industry has grown according to Moore's Law(Figure 1-1).

While Si-based transistors are dominant in market(over 90%) and continue growing, there are a lot of efforts in the development of compound semiconductor devices for optical devices, especially in the full range of wavelength, and for electronic devices operating at high frequency, high power, high temperatures, and harsh environments. Table 1-1 shows some unique properties of the compound semiconductor material systems. For ultra high speed application, gallium arsenide(GaAs) and indium phosphid(InP) have their merits due to much higher mobility than that of Silicon. In terms of thermal conductivity which is important for power devices, silicon carbide(SiC) and III-nitride are superior to Si. In addition, high breakdown field of both Silicon Carbide and III-Nitride make them the ideal candidates for the high breakdown voltage devices. Also, the extremely low intrinsic carrier concentration of wide bandgap semiconductors can lower the leakage current of transistors dramatically, as shown in Figure 1-2.

Another important application of semiconductors is optoelectronics for telecommunication, data storage and display areas. Since shortly after Thomas Edison demonstrated the incandescent electric lamp in 1879, light-bulb manufacture became a major industry. There have been big interests for more efficient and powerful light sources. After high efficient electro-luminescence from semiconductor devices was demonstrated in early 1960s[Bla63], light emitting diodes(LED) and laser diodes(LD) continue to experience strong growth.(Figure 1-3)

Most of LEDs are based on direct bandgap semiconductor systems(Figure 1-4). In most cases, these devices involve growing epitaxial layers of heterostructures by Molecular Beam Epitaxy(MBE), Chemical Vapor Deposition(CVD), and Vapor Phase Epitaxy(VPE). The opto-electronic devices based on AlGaAs/GaAs laser diodes are commercially used in the read/write heads of CD-ROM and DVD-ROM drives. By combining the red, green and blue color, any desired colors can be produced for full-colored light sources. Red traffic signals produced by filtering the red portion of incandescent wastes about 85% of the emitted light.[Pon97]. Most incandescent lamps have to be replaced a few times per year, but the lifetime of LEDs is over 5 years. Full-color LEDs can lower the cost in both energy and replacement. In addition to that, the stability of nitride materials is superior to other materials for outdoor applications. Some automobile companies started to install LEDs as interior panel lighting source.

1.2 Dissertation Outline

The literature review and background of wide bandgap semiconductors will be presented in Chapter 2. In Chapter 3, the fundamental current-voltage(I-V) and capacitance-voltage(C-V) measurement techniques using metal-oxide-

semiconductor(MOS) , and the demonstration of charge inversion using gate controlled diode structure employing MgO and Sc_2O_3 the gate will be discussed. Chapter 4 discusses the thermal stability of WSi_X and W Schottky contacts metallization on n-GaN, followed by the thermal stability of WSi_X in n-type 4H-SiC and the comparison of stability of WSi_X/SiC and Ni/SiC Schottky rectifiers to high dose gamma-ray irradiation. Chapter 5 describes the time response and temperature effect on the characteristics of Pt/4H-SiC gas sensors and the hydrogen sensitive GaN Schottky diodes. Chapter 6 presents a brief summary, including the conclusion and future work.

	Si (----)	GaAs (AlGaAs/ InGaAs)	InP (InAlAs/ InGaAs)	4H SiC (----)	GaN (AlGaN/ GaN)
Bandgap (eV)	1.1	1.42	1.35	3.26	3.49
Electron mobility (cm^2/Vs)	1500	8500	10000	700	900
Saturated (peak) electron velocity ($x10^7$ cm/s)	1	2.1	2.3	2	2.7
2DEG sheet electron density (cm^{-2})	NA	$<4 \times 10^{12}$	$<4 \times 10^{12}$	NA	$20x10^{12}$
Critical breakdown field (MV/cm)	0.3	0.4	0.5	2	3.3
Thermal conductivity (W/cm-K)	1.5	0.5	0.7	4.5	>1.7
Relative dielectric constant (εr)	11.8	12.8	12.5	10	9.0

Table 1-1 Selected material properties of Si, GaAs, InP, SiC and GaN semiconductors[Mor94]

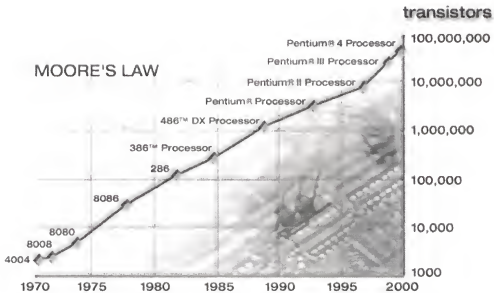

Figure 1-1 Moor's Law for Intel CPU from 1971 to 2000

[http://www.intel.com/research/silicon/mooreslaw.htm]

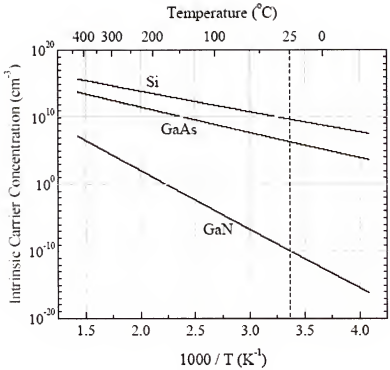

Figure 1-2 Intrinsic carrier concentration as a function of temperature for Si, GaAs, and GaN

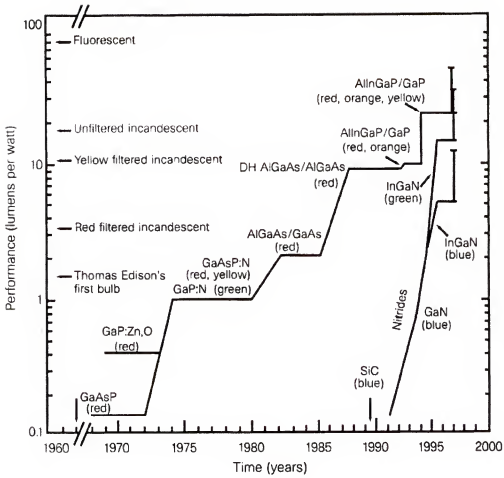

Figure 1-3 Evolution of LEDs.[Pon97]

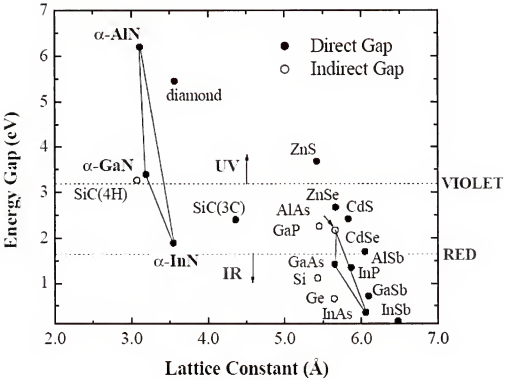

Figure 1-4 Energy bandgap diagram of compound and elemental semiconductors

CHAPTER 2
LITERATURE REVIEW AND BACKGROUND

2.1 Historical Review

Wurtizite GaN, aluminum nitride(AlN), and InN have direct bandgap energies of 3.4, 6.2 and 1.9eV, respectively(Figure 1-1)[Joh02], making nitride systems to be good candidates for LEDS, LDs, and detectors. Also, solid-state lighting can provide longer lifetime and lower power consumption compared with incandescent light source. [Nak95]. These achievements were made possible through several major breakthroughs. First, high-quality single crystal film was very difficult to grow due to no adequate substrate available. Sapphire and SiC are the typical substrate used for GaN epi-growth, however, the large lattice mismatches between GaN and the substrates limit the quality of GaN epi-layer. Recently researchers in Japan used AlN grown at low temperature as a buffer layer, which improved the crystal quality significantly[Amo98]. The n-type doping in GaN can be achieved using Si dopant. But p-type doping was still elusive until Akasaki et al. found Mg as a viable p-type dopant[Aka91]. Nakamura demonstrated the first GaN based blue LEDs, which were commercialized by Nichia in 1993, followed by Cree Inc, and LumiLeds Lighting. The first nitride diode laser was demonstrated in 1995 by Nakamura and coworkers at Nichia in 1993.

Another important application for the wide bandgap semiconductor is high power devices. Since wide bandgap semiconductor have high breakdown field, whihc is much higher than that of conventional Si and GaAs devices. A lot of progress has been made in the wide bandgap semiconductor based high power devices for the applications of

communication base stations, phased array radars, and satellite communication.[Zha03b]. AlGaN/GaN high electron mobility transistor(HEMT) with 70W CW operation at 2GHz was reported[Kik03]. AlGaN/GaN HEMTs are beginning to be commercialized, and SiC MESFETs based power Amplifiers are already in the market. GaN based rectifiers and field effect transistors are also very attractive for high temperature, high voltage, high power, and high frequency applications.

The remarkable growth of the IC industry has been indebted to the properties of SiO_2. Silicon dioxide can stand breakdown fields in the order of 1×10^7 V/cm with low interface state density on the order of low-middle 10^{10} /cm^{2}eV. However, unlike in Si technology, GaN does not have high quality native oxides. Almost all of GaN devices employ metal-semiconductor interface rather than insulator-semiconductor interface. In order to reduce the gate leakage current and increase device breakdown voltage, the metal oxide semiconductor (MOS) structure is preferred.

GaN MOS based diode or devices using AlN, $Ga_2O_3(Gd_2O_3)$, SiO_2, and Si_3N_4 as the gate oxides have been previously reported [Ale99, Aul98, Bin97a, Cas96b, Hon00c, Ren98a, Ren98b]. Various deposition techniques such as plasma enhanced chemical vapor deposition (PECVD), jet vapor deposition, MBE, MOCVD, and electron beam deposition were used for those oxide growths; however, no charge inversion was demonstrated. Recently the bixbyite oxide Gd_2O_3, grown via gas source molecular beam epitaxy on n-GaN, has been shown to achieve an interface state density of mid 10^{11} eV^{-1}cm^{-2}, but small energy bandgap of Gd_2O_3 (5.3 eV) limits the gate voltage swing.

The initial results for GaN-based MOSFETS were from Khan et. al.[Kha00], using a 13nm SiO_2 as the gate oxide to demonstrate AlGaN/GaN HEMTs. The device exhibited

remarkable results, the gate leakage current was lowered by six orders and higher linearity as compared to the Schottky based control sample. Another progress was from researchers in Taiwan.[Lee02] They used supersaturated hydrofluosilicic acid aqueous solution(H_2SiF_6) and boric acid aqueous solution(H_3BO_3) to deposit (.....nm) SiO_2 as the gate oxide with a rate of 50 nm/h at 40°C. This oxide exhibited a breakdown field in excess of 5MV/cm, which is half of that observed for SiO_2-Si interface. The interface state density was about $2\times10^{11}/cm^2eV$. The performance of GaN-based devices can be further improved by using different oxides and deposition techniques.

2.2 Background

2.2.1 Traps in device

In the MOS technology, the bulk oxide, the interface between insulator and semiconductor, and the semiconductor are three key regions, which will determine the performance of the devices. Traps forms in these three regions during oxide growth and device fabrication could cause a malfunction of the MOS device. Traps can be mobile ions, fixed oxide charges, and interface states.(Figure 2-2)

2.2.1.1 Mobile ions

The as-fabricated early Si-based MOS devices showed negatively-shifted C-V characteristics with respect to the theoretical curve.[Nic82] It was verified that the positively charged mobile ion(mainly Na^+) caused this phenomena due to alkali ions diffusing into oxide during the device fabrication.[Nic82] Mobile ions were eliminated by chlorine neutralization and phosphorus stabilization.[Nic82, Pie96]

2.2.1.2 Fixed oxide charge

Another contribution to the negative shift in the C-V, a few volts relative to the theoretical curve, is the fixed oxide charge. The fixed oxide charge was caused by a charge residing within the oxide close to the oxide-semiconductor interface. This charge is called built-in charge or oxide fixed charge. The oxide fixed charge is due to excess ionic silicons that have broken away from the semiconductor itself. The oxide fixed charges are mainly positive and immobile under an applied electric field. They do not exchange charges with the semiconductor biased at the different gate voltages.This effect was reduced by annealing the semiconductor in an inert atmosphere.[Pie96]

2.2.1.3 Interface trap

Interface traps, also known as the surface states, are energy levels in the band gap at the oxide-semiconductor interface. The levels of the surface states distributed throughout the bandgap. It is known that the interfacial traps in the upper half of the band gap are neutral when empty and negative when filled with an electron. When interface traps are present, the C-V response stretches out as compared to the theoretical C-V curve. The interface trap density is defined as the trap distribution in the bandgap(usually D_{it} with units of number/cm^2eV).(Figure 2-3)

The origins of the traps are believed that they are from unsatisfied chemical bondings (dangling bonds) at the surface of the semiconductor. For example, in Si surface, one of the four surface-atom bonds is left dangling, thus produces interface traps.(Figure 2-4)

Interface has traps distribute throughout the bandgap. However, these traps cannot communicate directly with each other and do not make an energy band. The interface also has oxide fixed charge as describe in the previous section. The interface trap density can be reduced by annealing in hydrogen ambient because hydrogen can passivate the dangling bonds.(Figure 2-5)

2.2.2 Interface trap density measurement techniques

2.2.2.1 High-low frequency capacitance-voltage method[Lay01a, Nic82, Sch98a, Sze81]

Castagne and Vapaille developed the high-low frequency capacitance-voltage method.[Cas71] The lower limit of surface state density stands around 10^{10} cm^{-2} eV^{-1} This approach seems simple, but it is very difficult to obtain low frequency C-V from wide bandgap semiconductors such as GaN, SiC, and AlGaN. This method is not valid for gate bias in or near inversion where minority carriers can not follow the high frequency gate bias.

The procedure of the high-low frequency capacitance-voltage method is described as following: first, collect the C-V data at high frequency, then measure the low frequency C-V data. The high frequency C_{OX} (which is oxide capacitance) in very strong accumulation coincides with the low frequency C_{ox} in very strong accumulation. If the series resistance is negligible,

At high frequency, $C_{HF} = \dfrac{C_s \cdot C_{ox}}{C_s + C_{ox}}$ so $C_s = \left(\dfrac{1}{C_{HF}} - \dfrac{1}{C_{ox}}\right)^{-1}$

Therefore, $C_{it} = \left(\dfrac{1}{C_{LF}} - \dfrac{1}{C_{ox}}\right)^{-1} - \left(\dfrac{1}{C_{HF}} - \dfrac{1}{C_{ox}}\right)^{-1}$

where C_{HF} is high frequency capacitance, C_{LF} is low frequency capacitance, Cs represents semiconductor capacitance, and C_{it} is interface capacitance.

2.2.2.2. Low frequency capacitance method[Nic82, Sch98a, Sze81]

Berglund developed the low frequency C-V method.[Ber66]. In very low frequency, it is assumed that the interface trap response is immediate with the bias.

$C_{it} = \left(\frac{1}{C_{LF}} - \frac{1}{C_{ox}} \right)^{-1} - C_s$ is the equation to extract the surface state density. A C-V data can be treated as a low frequency curve when the system is in thermal equilibrium during the measurement. For silicon based systems, frequencies of 1 Hz or below are usually chosen as low frequency.

For low frequency capacitance method, $\frac{dQ}{dt} = \left(\frac{dQ}{dV} \right) \cdot \left(\frac{dV}{dt} \right) = C \cdot \left(\frac{dV}{dt} \right)$ where Q is charge, V is bias, and t is time. The measurement is performed under equilibrium. The C-V curves which obtained with this method should have no hysteresis in both sweep directions.

2.2.2.3. High frequency capacitance method(Terman method)[Nic82, Sch98a, Sze81]

Terman developed the high frequency C-V method.[Ter62] The capacitance is measured as a function of gate bias with frequency fixed at a sufficiently high value (usually at 1 MHz) so that the interface traps and minority carriers cannot respond with the bias swing. Typically, , the minority carriers of the Si-based device cannot respond at the frequency above 1 kHz.

Although the interface traps cannot follow with ac gate voltage in the high frequency conditions, they can still follow the very slow changes of DC gate bias change. The interface traps can contribute the stretch-out of high frequency C-V data, but they do not contribute capacitance to the high frequency C-V curve. The key for the Terman method is to keep the frequency high enough so that the interface traps cannot follow. At the same time, the gate bias should be changed so slow that the interface trap occupancy can be changed.

The Interface traps produce a distortion in the shape of the C-V curve. The ideal C-V curve is calculated with the same oxide thickness and doping of the measured device without the interface traps.

At the high frequency condition, the total capacitance is given by $C_{HF} = \frac{C_s \cdot C_{ox}}{C_s + C_{ox}}$, since the frequency is too large for any ac response of interface traps. The high frequency capacitance of MOS capacitor should be same as that of the MOS capacitor without the traps, of only if C_s is same. C_S is the function of band bending. The band bending in ideal sample can be calculated. Theoretical φ_s(surface band-bending) should be related to experimental V_G to get all the information about interface density in high frequency C-V measurement.

Because C_{ox} can be measured and C_s depends on φ_s, ideal C_{HF} can be calculated. This plot can be compared with measured plot of C_{HF} versus gate bias. A qualitative relation of stretch-out by traps is

$$V_G = -\frac{Q_S}{C_{ox}} + \varphi_S - \frac{Q_{it}}{C_{ox}}$$

$$C_{ox}(V_G-\varphi_s)=-Q_{it}(\varphi_s)-Q_s(\varphi_s)$$

where Q_s is semiconductor surface charge per unit area.

$$C_{ox}dV_G - C_{ox}d\varphi_s = -dQ_{it}(\varphi_s) - dQ_s(\varphi_s) = C_{it}d\varphi s + Csd\varphi_s$$

where $Cit(\varphi_s) \equiv -dQit/d\varphi_s$ and $Cs(\varphi_s)) \equiv -dQs/d\varphi_s$

Therefore,

$$C_{it}(\varphi_s) = C_{ox}[(dV_G/d\varphi_s)-1] - C_s(\varphi_s) = qDit \text{ [Aru98]}$$

The plot V_G vs. C_{HF} from experiments can be generated, then plot φ_s vs. C_{HF} in theoretical method can be related.

2.2.2.4. AC conductance method[Ale98, Lay01a, Nic82, Sch98a, Sze81]

The ac Conductance method was proposed by Nicollian and Goetzberger.[Nic82] This technique is generally believed to be the most accurate method to extract D_{it}. The surface state densities can be measure as low as 10^9 $cm^{-2}eV^{-1}$. The changes in conductance and capacitance by this emptying and filling process of traps was measured.[Nic82]

The conductance loss, G_p/ω, was used to determine D_{it}. The measured admittance of the diode in depletion region determined the loss by the interface states traps.

The equivalent parallel conductance loss of interface traps is given by $\frac{G_P}{\omega} = \frac{\omega C_{ox}^2 G_m}{G_m^2 + \omega^2 (C_{ox} - C_m)^2}$ where ω is angular frequency, G_m represents measured conductance, G_p is conductance of interface traps, C_m represents measured capacitance, C_p is conductance of interface traps.

The interface trap density was calculated from

$\frac{G_P}{\omega} = \frac{q\omega\tau_{it}D_{it}}{1+(\omega\tau_{it})^2}$ where τ_{it} represents time constant of interface traps.

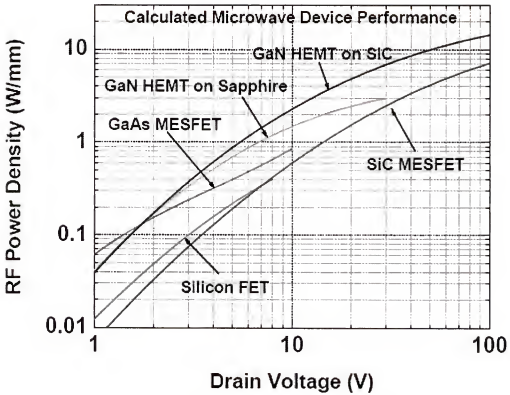

Figure 2-1 Calculated microwave device performance[Zha03a]

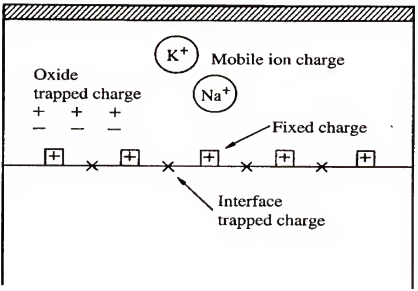

Figure 2-2 Traps in MOS structure[Pie96]

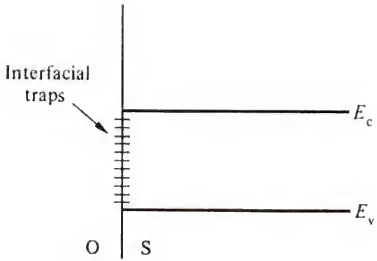

Figure 2-3 Interfacial Traps[Pie96]

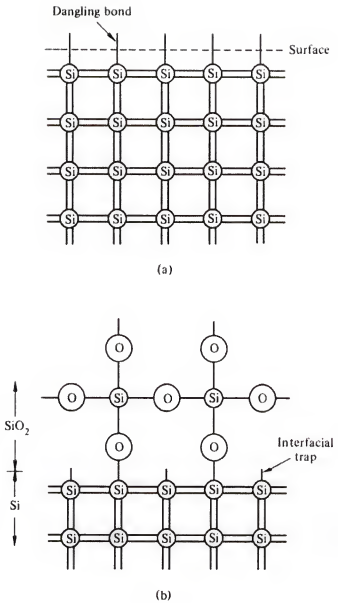

Figure 2-4 Origin of interfacial traps in SiO_2[Pie96]

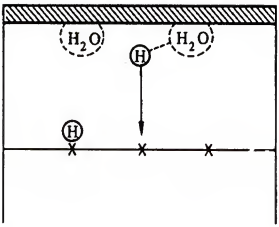

Figure 2-5 Passivation of interfacial traps[Pie96]

CHAPTER 3
GALLIUM NITRIDE BASED METAL-OXIDE-SEMICONDUCTOR DIODES

3.1 Introduction

There is great current interest in development of GaN-based metal-oxide-semiconductor(MOS) transistors because of their lower leakage currents and power consumption and capability for greater voltage swings relative to the more common Schottky-gate devices [Aru98, Bin97b, Cas96a, Che01, Fu02, Gil01, Has00, Hon00a, Hon00b, Hu01, Iro03, Iva01, Joh00, Joh01, Kah00, Kaw98, Kha00, Lay01b, Mis01, Mis02, Pea00, Ren98a, Ren98b, Tar03, The00, Zha00]. A wide variety of gate dielectrics for GaN have been reported, including oxides such as $Ga_2O_3(Gd_2O_3)$[Hon00a, Hon00b, Joh00, Ren98b], SiO_2[Che01, Has00, Iva01, Kha00, Kha00, Tar03, The00, Zha00], MgO[Gil01] and Sc_2O_3[Gil01] and insulators such as AlN[Hu01, Pea00] and SiN_x[Aru98, Bin97a, Iro03]. The deposition methods for these materials have included molecular beam epitaxy[Hon00a, Hon00b, Joh00, Joh01, Lay01b, Ren98a], plasma-enhanced chemical vapor deposition[Che01, The00], photoelectrochemical oxidation[Fu02, Mis01, Mis02] and e-beam evaporation[Hon00a, Hon00b, Lay01b].

The interface state densities derived from the Terman method[Ter62] are generally in the mid-to-high 10^{11} $eV^{-1}cm^{-2}$ range. Charge modulation from accumulation to depletion is commonly reported, but a clear demonstration of surface inversion has proven elusive due to the very low minority carrier generation rate in GaN at room temperature.[Hon01] Even at 300°C in conventional GaN MOS devices, the generation

rate is still too low to observe inversion. To overcome a similar problem in SiC MOS devices, the n^+p junction of a MOS gate-controlled device was employed as an external source of the inversion charges[She94].

The most widely studied GaN-based electronic device is the AlGaN/GaN HEMT, in which current flow is typically controlled by a Schottky metal gate[Bin97b, Dau99, Eas01, Gre00, Hu01, Kha00, Koh99, Lee01a, Lu01, Ngu00, Ngu99, Sim00, Tar01a, Wu97]. There is also interest in developing gate dielectrics for GaN, which allow for metal-insulator-semiconductor(MIS) or metal-oxide-semiconductor(MOS) controlled transistors [Aru98, Bin97a, Gaf01, Has00, Iro03, Joh00, Joh01, Kha01, Lay01b, Ren98b, Sim01, The99, Zha00]. The advantage of MOS or MIS GaN-based transistors would be the possibility of using the gate oxide/insulator material as a surface passivation film[Tar01a]. Current state-of –the-art AlGaN/GaN HEMTs generally show a decrease in drain current at high drain-source voltage[Bin01, Eas01]. This collapse of the current produces a severe degradation of the RF output power. One of the main mechanisms for the phenomena is the presence of surface states in the region between the drain and source. The use of SiN_x passivation layers on top of the AlGaN/GaN structure helps to partially mitigate the current collapse [Bin01, Eas01, Gre00, Lee01a].

It is believed that oxides such as Sc_2O_3 and MgO are effective in reducing the effect of surface states on AlGaN/GaN HEMTs and, in addition, exhibit promise as gate dielectrics in GaN.[Gil01, Luo02a, Luo02b] In particular, the Sc_2O_3 produces more stable passivation of the GaN surface than MgO. The Sc_2O_3 had a bixbyite crystal structure, with a 9.2% lattice mismatch to GaN, a high dielectric constant[Tar01b] and reasonable bandgap(6.3eV).

3.2 Molecular Beam Epitaxy Oxide Growth

Oxide growth was performed in a RIBER 2300 MBE equipped with a reflection high-energy electron diffraction (RHEED) system. Figure 3-1 illustrated the overview of MBE system used to grow oxides. Substrates employed were MOCVD grown n-GaN on sapphire (0001). Oxygen was supplied from a Wavemat MPDR 610 electron cyclotron resonance (ECR) plasma source (2.54 GHz) with 200W forward power at $1x10^{-4}$ Torr of the oxygen pressure. A standard effusion cell operating at 1130°-1170°C was used for the evaporation of the magnesium. The substrate temperature was kept at 600 °C and measured using a backside thermocouple that was calibrated using the melting points of InSb and GaSb.

Prior to the oxide growth, the GaN substrate preparation consisted of a wet chemical etch of $HCl:H_2O$ (1:1) for 3 minutes, a DI rinse, a UV-ozone exposure for 25 minutes in a UV Cleaner model 42-220, a dip in buffered oxide etch (6:1, ammonium fluoride : hydrofluoric acid) for 5 minutes and a final DI rinse. The substrates were then indium mounted to molybdenum blocks and loaded into the MBE. At room temperature the surface of the substrates was polycrystalline according to the RHEED patterns. Upon heating the GaN to 700°C, a streaky (1×3) pattern appeared. This was the starting surface for all the films grown in this dissertation.

3.2.1 Growth of MgO on GaN

The MgO was deposited by MBE at 100°C on a GaN layer grown by metal organic chemical vapor deposition on sapphire. The MgO precursors were elemental Mg and radio-frequency plasma-activated oxygen. The samples were then loaded into the MBE

system and heated at 650°C to ensure oxide removal. A standard effusion cell operating at 380°C was used for evaporation of the Mg, while the O_2 source was operated at 300W forward power(13.56MHz) and 2.5×10^{-5} Torr.

3.2.2 Growth of Sc_2O_3 on GaN

The starting sample was a 1μm thick GaN layer grown on a 2 μm undoped GaN buffer grown on a Al_2O_3 substrate by MOCVD. The Sc_2O_3 was deposited by rf plasma-activated MBE at 650°C using elemental Sc evaporated from a standard effusion cell at 1130 °C and O_2 derived from an electron cyclotron plasma source operating at 200W forward power(2.45GHz) and 10^{-4} Torr.

3.3 GaN Based MOS Diode Fabrication

3.3.1 MgO/n-GaN MOS Diode Fabrication

The diode fabrication started with ohmic contact formation by removing either MgO or Sc_2O_3 and depositing Ti/Al/Pt/Au. AZ1045 was used as etch mask. The MgO was removed by wet etching in a H_3PO_4 solution while Sc_2O_3 was dry-etched in an inductive coupled plasma(ICP) system. A standard lift-off process was employed for the Pt/Au based gate deposition. Figure 3-2 illustrates a cross-section view of the diode. Figure 3-3 shows TEM pictures of MgO.

3.3.2 MgO/p-GaN Gate-Controlled Diodes Fabrication

Multiple energy of of 70, 195, 380 keV $^{29}Si^+$ ion implantation with doses of 2×10^{13}, 6×10^{13}, $1.8 \times 10^{14} cm^{-2}$, respectively, used to create the n^+ gate-contact regions followed

by high temperature(~950°C) activation annealing.. The MgO was then removed in all areas except for the gate region, using H_3PO_4 etchant and an AZ-1045 resist mask. The e-beam deposited Ti/Al/Pt/Au andPt/Au metallizations were used for n- and p-ohmic contact, respectively, with the standard lift-off process. Pt/Au metallization was used of rhte gate contacts. A schematic of the final structure is shown in Figure 3-7 and a microscope image is shown in Figure 3-8.

3.3.3 Sc_2O_3/p-GaN Gate-Controlled Diodes Fabrication

The Sc_2O_3 layers were ~400Å thick. N^+ regions were created by selective implantation of Si^+ with multiple energies and doses (70keVof $2x10^{13}cm^2$, 195 keV of $6x10^{13}cm^{-2}$ and 380 keV of $1.8x10^{14}cm^{-2}$). The samples were then annealed at 950°C under N_2 to activate the Si-implanted regions. Contact windows were etched into the oxide and e-beam deposited p-ohmic(Ni/Au), n-ohmic(Ti/Al/Pt/Au) and gate metal(Pt/Au) were formed with t he standard lift-off process. The separation of the n^+ regions was ~ 60μm. A schematic of the completed gate-controlled diode is shown in Figure 3-12.

Capacitance and conductance measurements were performed with an HP 4284 precision LCR meter. A hot chuck was used for the high temperature conductance measurements and the temperature range was from room temperature to 300 °C.

3.4 Diode DC and AC Characteristics

3.4.1 MgO/n-GaN MOS Diodes

Figure 3-4 shows the I-V characteristics at 25° C from a MgO/GaN diode with 100 nm MgO gate dielectric. The reverse breakdown and forward turn-on voltage are >40 V and >10 V, respectively, where these parameters are defined as the values at 100 nA or 5 mA/cm^2). A forward breakdown field of 1.2 MV/cm for MgO was calculated based on this data.

The measured C-V curve at a frequency of 1 MHz and sweep-rate of 100 mV/s, as illustrated in Figure 3-5, showed a clear deep depletion behavior at the negative bias voltage region and no measurable hysterisis was observed. The deep depletion feature with no inversion capacitance characteristics is typical of the wide-gap semiconductor MIS structures due to the slow generation rate of the minority carrier at room temperature. Using the relation of $C_{ox} = \varepsilon_o \varepsilon_{ox} A/T_{ox}$, the dielectric constant of the oxide, ε_{ox}, was calculated to be 10.5, which is in agreement with the tabulated value for MgO (9.8). The interface state density was calculated using the Terman method to be $4 \times 10^{11} eV^{-1} cm^{-2}$ at 0.3 eV below the conduction band edge, as shown in Figure 3-6. The Terman method provides a rough evaluation of MgO/GaN interface trap density. It is based on the extraction of the experimental surface potential, ψ_s, versus gate voltage, V_g. The measured C-V curve stretched out away from the theoretical C-V curve, which leads to the determination of interface trap density. The Terman method is generally found to underestimate the trap density[Lay01a].

The conductance technique was also used to characterize the MgO/GaN MOS capacitors. The admittance of the MOS capacitor measured is $G_m + j\omega C_m$, where G_m is measured equivalent parallel conductance, ω is the angular frequency, and C_m is the measured capacitance. Converting the admittance to an impedance, subtracting the reactance of the oxide capacitance, and converting back to an admittance yielded for the real part

$$\frac{G_P}{\omega} = \frac{\omega C_{ox}^2 G_m}{G_m^2 + \omega^2 (C_{ox} - C_m)^2}$$

where C_{ox} is measured in strong accumulation[12]

The width of the G_p/ω versus log (ω) curve depends only on the band-bending. The G_p/ω versus gate bias curve will be spread over a bias range determined by band-bending and D_{it}. For each G_p/ω curve, the standard deviation of band-bending, σ_s, can be obtained. The D_{it} were calculated with

$$D_{it} = \left(\frac{Gp}{\omega}\right)_{f_p} \left[q f_D(\sigma_S) A\right]^{-1}$$

where f_D is a function depending on σ_s, A is the area of diode, and f_p is the frequency at the maximum number of G_p/ω. The values for f_D from our samples ranged from 0.35 to 0.4. The estimated interface trap density is illustrated in Figure 3-6 along with the results obtained from Terman method. An interface state density of 4×10^{11}/eV.cm^2 at E_c-E_t = 0.3 eV was obtained, which was slightly higher than that of Terman method. The Terman method provides a rough evaluation of MgO/GaN interface trap density and in general underestimates of the trap density are expected[Nic82]. Though the Terman method underestimates interface state density, its value is reasonable near the conduction band edge.

3.4.2 MgO/GaN Gate-Controlled MOS Diodes

Room temperature C-V characteristics from a 40 μm diameter oxide contact MOS diode are shown in Figure 3-9. Deep-depletion characteristics and no inversion behavior were observed, even for measurement temperatures up to 300°C. In addition, the diode exhibited good rectification, demonstrating that MgO produces excellent insulator characteristics. The reverse breakdown of the diode with as-deposited dielectric was ~12V, with a forward turn-on voltage of ~10V. By sharp contrast, if the Pt/Au was placed directly on the p-GaN without any MgO, the forward turn-on voltage was <0.7V and the reverse breakdown voltage was <1V. The forward breakdown field prior to annealing was ~1.2 $MVcm^{-1}$ for the MgO, where breakdown was defined as the voltage at which the forward current density is 5 $mA\text{-}cm^{-2}$.

Figure 3-10 shows C-V characteristics of the MgO/GaN MOS-controlled diodes at 25°C in the dark as a function of the measurement frequency. In each case, -20V was applied at the gated contact to provide a source of minority carriers. The frequency dispersion observed in inversion is due to the resistance of the inversion channel, as reported for n^+p SiC MOS gate-controlled diodes.[She94] At 5KHz measurement frequency, only deep depletion was observed since the characteristics are dominated by majority carriers[Goe68]. As the frequency is decreased, a clear inversion behavior is observed due to charge flow into and from the n^+ regions external to the gate. It is likely that many of the gate oxides reported for GaN would also be capable of producing inversion behavior in MOS structures if a gated-contact were included.[Che01, Mis01, Mis02] As mentioned above, in diodes without the n^+ regions to act as an external supply

of minority carriers, inversion could not be observed, even up to measurement temperatures of 300C.

Figure 3-11 shows I-V characteristics from the diodes at 25°C in the dark. For the accumulation region at negative bias, the reverse current is mainly due to diffusion and generation in the depletion region. As the bias is moved to positive values, the current increases due to the presence of two additional components; namely the additional depletion region under the gate provides more gate current and the surface generation current increases. As the bias is further increased to the inversion region, this surface generation component is suppressed, leaving only the current due to generation in the depletion region. This is the classical behavior for a gate-controlled diode.

Clear inversion in MgO/p-GaN MOS diodes at 25°C in the dark by employing n^+ drain regions as a source of minority carriers have been demonstrated. This provides a solution to the very low generation rate of minority carriers in GaN at room temperature. The MgO produces a relatively low interface state density on GaN and is stable against activation annealing for the implanted n^+ regions in the MOS gate-controlled diodes. This dielectric looks very promising for realization of enhanced-mode GaN MOS transistors.

3.4.3 Sc_2O_3/GaN Gate-Controlled Diodes

A Sc_2O_3/p-GaN MOS diode without the n^+ regions to provide an external source of minority carriers cannot remain in thermal equilibrium as the applied gate bias is swept from negative to positive polarity because of the extremely low minority carrier generation rate in the wide bandgap (3.4eV) GaN. Examples are shown in Figure 3-13, where only deep-depletion characteristics are observed, even up to a measurement

temperature of 300°C. Achievement of inversion is not possible due to the low concentration of thermally generated electrons.

Figure 3-14 shows the C-V_G characteristics for various biases on the n^+p junction diode. There are several key features of the data. Firstly, a clear inversion behavior is observed as electrons supplied from the n^+ regions are drawn into the gate. Secondly, when the n^+p junction is reversed-biased, the onset of inversion is delayed, as demonstrated by the threshold voltage shift apparent in the C-V curves. This is the classical behavior experienced for a gate-controlled MOS diode.[Sch86] Thirdly, the presence of a hook region in the C-V curve is caused by a surface-state-induced barrier against electron flow at the boundary of the MOS diode. This type of behavior has been reported previously for both SiC[Goe68] and SiC[She94] gate-controlled diodes and results from the nonequilibrium characteristics of deep level surface traps on the semiconductor. The total concentration of surface states, N_{SS} can be obtained from the relation[Gro66]

$$N_{SS} \sim (\Delta V.C_0)/e$$

where ΔV is the voltage difference between the two minima in the characteristic obtained with a grounded n^+ region, C_o is the Sc_2O_3 capacitance under the gate and e is the electronic charge. From Figure 3-14, N_{SS}~$8.2x10^{12}cm^{-2}$, which is approximately a factor of two higher than for comparable SiO_2/SiC diodes reported previously[She94]. At 200KHz, gate-controlled diode also showed inversion behavior, as shown Figure 3-15.

The frequency dependence of the C-V characteristics for grounded gate contact conditions is shown in Figure 3-16. Inversion is obtained at 25°C for a measurement frequency of 150kHz, while the accumulation capacitance exhibits a strong dependence

of frequency with roughly a factor of two difference when the frequency is decreased from 1 MHz to 150kHz. A similar phenomena has been reported for MIS capacitors on Si using $SrTa_2O_6$ or $ZrSiO_4$ gate dielectrics.[Jia03] For our structures, the accumulation capacitance dependence on measurement frequency can be represented by the relation,

$$C_p = \frac{C_O}{1 + \omega^2 R_S^2 C_O^2}$$

where C_p is the measured capacitance and R_S is the total resistance. To explain the data in Figure 3-16, it is thought that there is an interfacial layer between the stoichiometric Sc_2O_3 and p-GaN produceing an impedance contribution. The resistance of the interfacial layer is assumed to decrease with frequency due to an increase in hopping conductance and this produces the observed decrease in accumulation capacitance with increasing measurement frequency[Jia03].

N^+p gate-controlled diodes have been demonstrated in GaN using novel gate dielectric materials and selective implantation. The total surface state density was estimated to be 8.2×10^{12} cm^{-2} from the drain-voltage dependence of the C-V characteristics. The presence of the surface state is manifested by a hook shape in the C-V curves. The use of the n^+ drain regions is effective in overcoming the low minority carrier generation rate in GaN and provides a source of inversion charge.

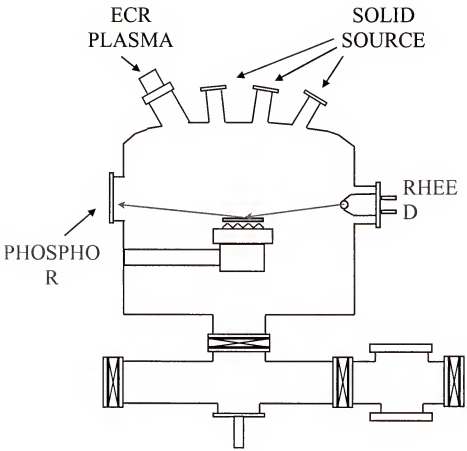

Figure 3-1 The overview of MBE system

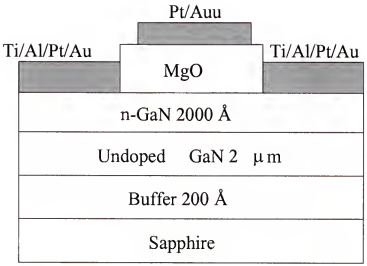

Figure 3-2 Cross-sectional view of a GaN diode with MgO as the gate oxide

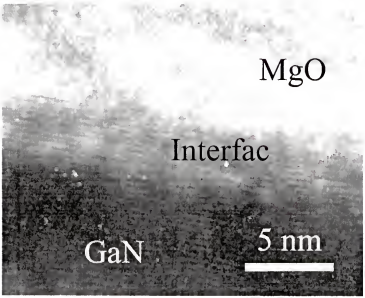

Figure 3-3 TEM picture of MgO/GaN sample

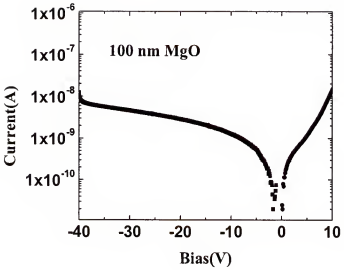

Figure 3-4 Diode characteristics of a 100 nm thick MgO/GaN diode

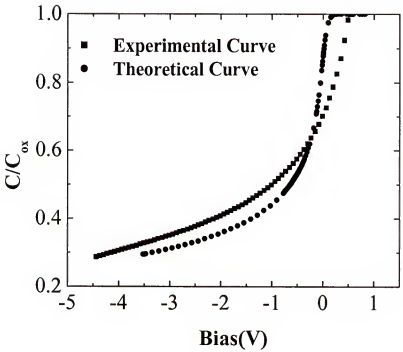

Figure 3-5 Typical C-V curve of a MgO/GaN diode under dark conditions at room temperature

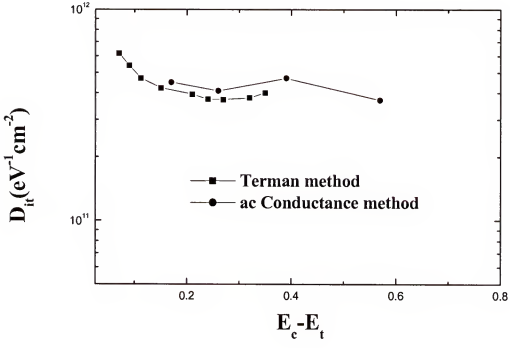

Figure 3-6 Interface trap density distribution close to the GaN conduction band obtained on a MgO/GaN MOS diode

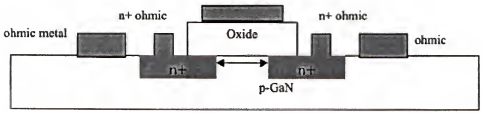

Figure 3-7 Schematic cross-section of n+p GaN MOS gate-controlled diode(top) and SEM plan view of device layout

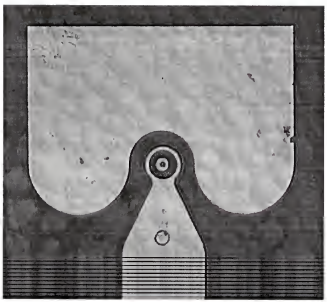

Figure 3-8 Microscope View of device layout

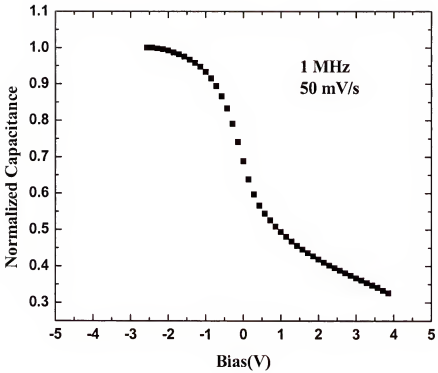

Figure 3-9 1MHz C-V characteristic at 25°C of 40 μm diameter Pt/Au contact ,conventional MgO/p-GaN diode without any n^+ region to act a source of minority carriers

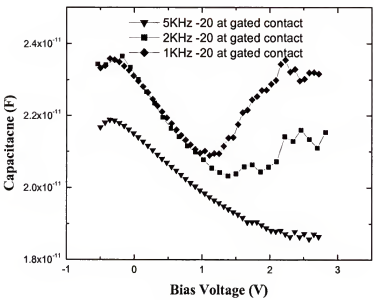

Figure 3-10 C-V characteristics of GaN MOS gate-controlled diodes at 25°C as a function of measurement frequency(+15V bias in gated contact in each case).

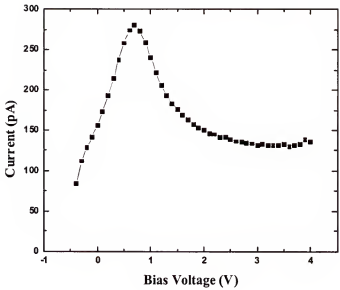

Figure 3-11 I-V characteristics of GaN MOS gate-controlled diodes at 25°C ,showing regions due to inversion(bias>2 V) and depletion(bias~ 0.75 V).

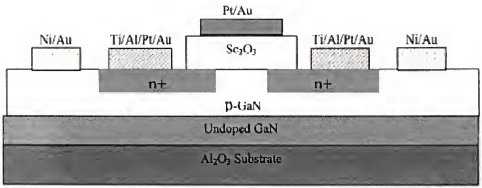

Figure 3-12 Schematic of Sc_2O_3/p-GaN gate-controlled diodes

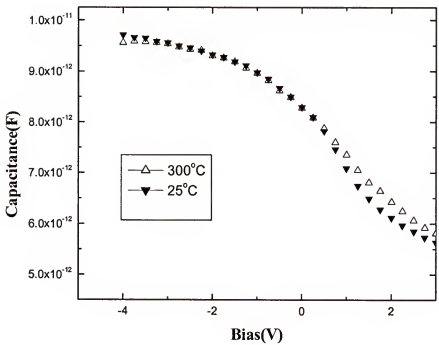

Figure 3-13 Temperature dependence of 150 kHz C-V characteristics for ungated Sc_2O_3/p-GaN MIS diodes without source of minority carriers.

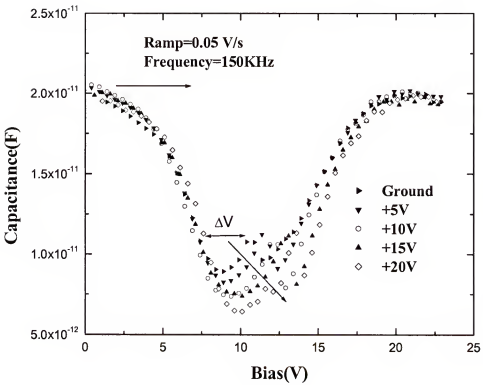

Figure 3-14 C-V characteristics of Sc_2O_3/p-GaN gated diodes as a function of drain bias at 25°C in the dark. The voltage ramp rate was 0.05 $V \cdot s^{-1}$ and measurement frequency 150kHz

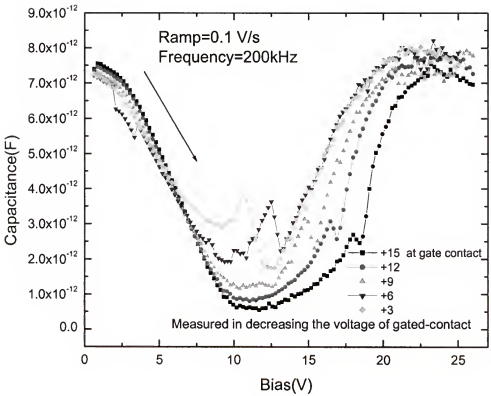

Figure 3-15 C-V characteristics of Sc_2O_3/p-GaN gated diodes as a function of drain bias at 25°C in the dark. The voltage ramp rate was 0.1 $V \cdot s^{-1}$ and measurement frequency 200kHz

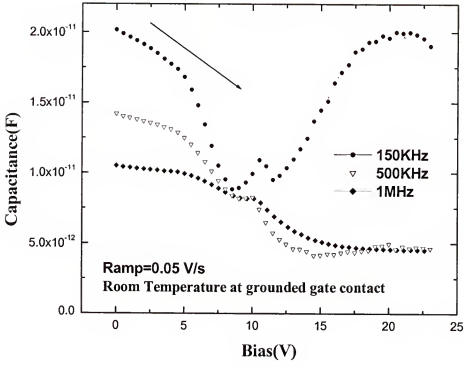

Figure 3-16 C-V characteristics of Sc_2O_3/p-GaN gated diodes as a function of measurement frequency at 25°C. The voltage ramp rate was 0.05 $V \cdot s^{-1}$ and there was zero drain bias

CHAPTER 4
SCHOTTKY METALLIZATION ON WIDE BANDGAP SEMICONDUCTORS FOR THE APPLICATIONS IN HARSH ENVIRONMENT

4.1. Introduction

There is a strong interest in developing thermally stable rectifying contacts in n-GaN and SiC for applications such as high power rectifiers for utility and for combustion gas sensors in long-duration space flights[Bra99, Cao99, Che02, Col96, Has02, Hsu01, Ish98, Kar00, Kok01, Liu70, Liu98, Maf02, Mo98, Moh96, Pea99, Pin96, Ric02, Sch02, Sch98b, She98, Ven98, Wan96, Yu98, Zha01, Zho02]. Past works in Schottky contacts in GaN are the importance of surface cleanliness prior to metal deposition[Cao99, Liu21, Moh98], the presence of strong spatial non-uniformities in reverse current[Bra99, Hsu01, Moh98], the influence of crystal polarity in barrier height[Kar00] and the presence of leakage current well in excess of those expected from thermionic emission[Bra99, Cao99, Che02, Col96,Has02, Hsu01, Ish98, Kar00, Kok01, Liu70, Liu98, Maf02, Mo98, Moh96, Pea99, Pin96, Ric02, Sch02, Sch98b, She98, Ven98, Wan96, Yu98, Zha01, Zho02]. It has also been noted that metal silicides are ideal candidates as thermally stable rectifying contacts due to the generally higher inertness of the silicide/GaN interface relative to pure metal layers[Liu97]. W and WSi_X have shown excellent thermal stability as ohmic contacts in n- and p-type GaN[Cao98, Col96, Col97], with limited reaction between the metals and the semiconductor up to ~1000°C. The formation of β-W_2N and W-N interfacial phases were deemed responsible for the electrical properties after these high

temperature treatments[Col96, Col97]. However there is no investigation of the use of these metals as Schottky contact in GaN.

SiC rectifiers are alternative for many applications, including inverters in utility power flow control, traction motor control and combustion gas sensing[Ale01, Alo97, Cas00, Cas98, Kni02, Mor01, Pet97, Sax99, Sin02a, Tar02, Tob97, Tri99]. The wide bandgap (3.2eV) and high band-strength(eV/atom) of 4H-SiC suggest it is a promising candidate for sensors and high temperature electronics in the nuclear power industry and satellite-based systems[Cas00, Cas98, Shu98]. This has stimulated interest in understanding the electrical properties and thermal stability of metal contacts on SiC[Col00, Col02, Cro97, Ito97, Kes00, Lee00, Lee01b, Luc01, Lun00, Lun96, Mel97, Mok98, Ode98, Osk00, Por95, Sax99, Sch98b, Skr00, Wal92, Zee02]. In particular, systems such as WC[lun00], Ti0.58W0.42[Lee00] and Pt/Ti/WSi/Ni[Osk00] show very promising stability on SiC for high temperature applications. The WC showed a relatively low barrier height of 0.79eV at 300K in n-type 6H-SiC[Lun00], while Ti0.58W0.42 showed a higher value of 1.22eV in n-type 6H-SiC over the temperature range 24~300°C[Lee00]. Pt/Ti/WSi/Ni contact on n-type 6H-SiC annealed at 1000°C showed excellent long-term stability as an ohmic contact [Osk00].Sputtered WSi0.45 showed a barrier height of 1.15eV after a 500°C post-deposition annealing treatment and retains a barrier-height of ≥1eV to anneal temperatures above ~700°C. The thermal stability is better than that of Ni, which is a very common Schottky metallization for 4H-SiC.

SiC Schottky rectifiers have shown exceptional radiation hardness to high energy(40MeV) protons typical of those encountered in the upper atmosphere[Nig02].

However, initial results on high dose gamma-ray irradiation, particularly of Ni/SiC Schottky rectifiers[Kim03b], have shown significant degradation of the forward current characteristics, due mainly to instability of the contacts[Kim03b].

4.2 Schottky Diode Processing

4.2.1 WSi_X/GaN Schottky Diode

The GaN samples were ~6μm of n-type($10^{17}cm^{-3}$)GaN grown on sapphire substrates with a hydride vapor phase epitaxy system. Electron-beam deposited Ti/Al/Pt/Au ohmic contacts were patterned by lift-off and annealed at 700°C for 30 secs under a flowing N_2 ambient. 700Å of W or $WSi_{0.45}$ layer was deposited using an Ar plasma-assisted sputtering system. Prior to sputtering, the GaN native oxide was removed by rinsing the samples in both a 20:1 H_2O:NH_4OH solution and buffered oxide etchant(BOE). To reduce the sheet resistance of the contacts, a bilayer of 200Å Ti/800Å Au was deposited on the W or WSi by e-beam evaporation. The diameter of Schottky diode was 120μm. The thermal stability of the diodesamples were annealed at different temperatures up to 700°C for 1 min under flowing N_2 for the thermal stability study. Current-voltage(I-V) measurements were performed at 25°C using an HP4156C parameter analyzer.

4.2.2 WSi_X/SiC Schottky Diode

Approximately 10μm of undoped($n\sim2\times10^{15}cm^{-3}$) was grown on n^+($n\sim10^{19}cm^{-3}$) 4H-S substrates with a vapor phase epitaxy system. E-beam evaporated Ni(200nm) was

deposited for full backside area ohmic contact and was annealed at 970°C for 3mins to achieve a low resistance ohmic contact. The samples were cleaned sequentially in acetone, iso-propanol and BOE prior to sputter deposited700Å of $WSi_{0.45}$ using an Ar plasma and separate W and Si targets. The 120μm diameter Schottky diodes were patterned using standard photolithography processing. Diodes with e-beam evaporated Ni Schottky contacts were also fabricated as the reference sample. The thermal stability of the WSi_X diodes were tested for anneals them up to 1100°C for 1 min under flowing N_2 in a Heatpulse 610T furnace. Current-voltage (I-V) measurements were performed in the temperature range of 25~300°C using an HP4156C parameter analyzer.

4.2.3 Gamma-Ray Irradiation to Schottky Diodes

The WSi/SiC and Ni/SiC Schottky diode samples were exposed to different doses of Co-60 γ-irradiation. Current-voltage(I-V) characteristics before and after irradiation were obtained at 25°C using a HP 4145 parameter analyzer. A schematic of the completed devices is shown in Figure 4-8.

4.3 Results and Discussion

4.3.1 WSi_X/GaN Schottky Diode

For the case of thermionic emission dominating the current transportation, the forward current density, I, of the Schottky diode can be expressed as

$$I = I_S \exp\left[\frac{e(V - IR)}{nkT} - 1\right]$$

where $I_S = AA^{**}T^2 \exp\left(\frac{e\phi_B}{kT}\right)$, I_S is the saturation current, e the electronic charge, V the applied voltage, R the series resistance, n the ideality factor, k is Boltzmann's constant, T is the measurement temperature, A the contact area, A^{**} is Richardson's constant for n-GaN and ϕ_B is the field-sensitive barrier height [Liu97]. For W on GaN, the theoretical barrier-height extracted from the relation $\phi_B=\phi_m-\chi_S$, where ϕ_m is the metal work function and χ_S the electron affinity of GaN is 0.4eV[Zei00]. The forward I-V characteristics of W/GaN diodes shown at the top of Figure 4-2 could not be fit to the thermionic emission relation for any of the conditions employed here, suggesting the presence of other current transport mechanisms such as tunneling through deep levels, surface leakage and space-charge generation. Evidence for this assertion comes from the reverse current characteristics shown at the bottom of Figure 4-2, where for the as-deposited diodes and these samples annealed up to 600°C. The reverse current density was found to vary approximately as the square root of the reverse bias, indicating that a space-charge generation current may be present. Upon annealing at 700°C, previous results suggest the onset of β-W_2N formation is responsible for the poorer rectifying behavior[Col96].

The corresponding I-V characteristics for WSi_X/GaN diodes are shown in Figure 4-3. In this case there was a reasonable range of forward characteristics[Ric02], producing the barrier height shown in Table 4-4. As pointed out previously, ϕ_B extracted from I-V measurements is field-dependent and can be related to a zero-field barrier height ϕ_F through the relationship[Liu97, Wag83].

$$\phi_F = n\phi_B - (n-1)\frac{kT}{e}\ln\frac{N_c}{N_d}$$

where N_c is the effective density of states in the conduction band and N_d is the donor concentration in the GaN. Table 4-4 also shows the extracted ϕ_F values, which are ~0.1eV lower than those of ϕ_B. This difference is consistent with that reported previously for PtSi Schottky contacts in n-GaN[Liu97].

In the presence of image-force induced barrier lowering, the reverse current can be expressed from equation[Ric02] as $I_R = AA^{**}T^2 \exp\left[\frac{e}{kT}(\phi_B - \Delta\phi_B)\right]$

where $\Delta\phi B$ is the image force barrier lowering.

The reverse current shown in Figure 4-3(bottom) is several order of magnitude higher than expected from equation[Pin96] and indicating that mechanisms such as field emission edge or surface leakage, depletion layer generation or defect-assisted tunneling are present. Detailed analysis of Ni and Pt/n-GaN Schottky diodes also showed high reverse leakage currents, which were modeled in focus of the presence of a high density of vacancies[Has02]. In this case such donors could result from the energetic ion bombardment of the surface during the sputter deposition process.

4.3.2 WSi_X/SiC Schottky Diode

Figure 4-4 shows the forward(top) and reverse(bottom) I-V characteristics for WSi_X diodes as a function of post-deposition annealing temperature. The as-deposited diodes show signatures of sputter-induced damage causing a high series resistance. The average energy of incident Ar^+ ions on the SiC sample is ~100eV, but this is sufficient to cause displacement damage in the semiconductor. The post-deposition annealing appears effective at recovering this ion-induced damage. For anneals at ≥900°C, the diodes show

high forward and reverse current which is indicative of a reaction between the WSi and the SiC, lowering the effective barrier height.

The current density J for a Schottky diode can be written

$$J = J_S\left[\exp\left(e\frac{V - J_{RON}}{nkT}\right) - 1\right]$$

where the saturation current density J_S is given by

$$J_S = A^{**}T^2\exp\left(-\frac{e\phi_B}{kT}\right)$$

where A^{**} is the Richardson's constant(146 $A{\cdot}cm^{-2}K^{-2}$ for SiC), T is the absolute measurement temperature, e the electronic charge, k is Boltzmann's constant, V the applied voltage, n the ideality factor and R_{ON} the on-state resistance. From the linear portions of the forward I-V characteristics in Figure 4-5, the barrier height was extracted for the WSi_X contacts and also the ideality factors as a function of post-deposition annealing temperature from the relations

$$\phi_B = \frac{kT}{e}\ln\left(\frac{A^{**}T^2}{J_S}\right)$$

$$n = \frac{e}{2.3kT}\left(\frac{\partial V}{\partial \log(J)}\right)$$

The resulting values are summarized in Table 4-2. The as-deposited contacts show an ideality factor of ~2, which is indicative of the presence of a high density of recombination centers. The 500°C anneal treatment increases the barrier height and decreases the ideality factor. This appears to be the optimum conditions for maximizing the barrier height. For comparison, Ni deposited on the same wafers showed a slightly lower ϕ_B(1.1eV) and higher ideality factor, as also shown in Table 4-2. By comparison,

Ti shows a ϕ_B of ~0.8eV in n-type SiC, Au has ~1.7eV, TiW has 1.2eV and Pt has 1.4eV. Annealing at ≥900°C severely decreases the barrier height and also degrades the ideality factors of the WSi_X contacts.

Figure 4-6 shows the forward I-V characteristics from Ni and WSi_X contacts in SiC, as a function of measurement temperature. The WSi_X sample was annealed at 500°C prior to the measurements. As is seen by comparing the magnitude of the currents at a given forward bias, the WSi_X has slightly lower current, particularly at higher measurement temperature. This suggests that this metallization system has a barrier height that decreases less with temperature than Ni does, and this would be an advantage in high temperature applications. This is confirmed by the data in Table 4-3, which shows ϕ_B and n for both the WSi_X and Ni contacts as a function of measurement temperature. Future work will focus on measuring the barrier height of WSi_X in p-type 4H-SiC in order to see if the sum of ϕ_{Bn} and ϕ_{Bp} are in good agreement with the temperature dependence of the bandgap.

$E_g(T)= 3.0-3.3x10^{-4}$ (T-300K) for 4H-SiC[Lee00]

In the case it would prove that the WSi_X contacts obeyed the Schottky-Mott- model in which ϕ_{Bp} would be given by $E_g-(\phi_m-\chi_s)$[Mel97].

Figure 4-7 shows the reverse I-V characteristics from both Ni(top) and WSi(bottom) contacts on 4H-SiC, as a function of measurement temperature in the range of 25~300°C. The range of reverse current magnitudes is comparable at high bias, although once again the WSi_X contacts have lower currents at small bias and elevated temperature(300°C) which should be an advantage in high temperature applications.

4.3.3 Comparison of Stability of WSix/SiC and Ni/SiC Schottky Rectifiers to High Dose of Gamma-Ray Irradiation

Forward current density versus voltage characteristics of both Ni/SiC and WSi_X/SiC rectifiers before and after γ-irradiation to different doses are shown in Figure 4-9. Prior to irradiation the barrier heights for the two types of diodes were 1.17eV(WSi_X) and 0.95(Ni), while the reverse breakdown voltage(V_B) were ~450V for Ni and ~408V for WSi_X. The typical on-state resistance, R_{on}, where R_{on} is given by[Sin02b] $4V_B/\mu\varepsilon E_C^3$(where μ is the electron mobility, ε the permittivity and E_C the critical field for breakdown), was 0.8 $m\Omega cm^2$ for Ni and 0.7$m\Omega cm^2$ for WSi_X. After irradiation there was a slight increase in series resistance in the WSi_X/SiC rectifiers, which is consistent with a reduction in carrier density in the depletion region through the introduction of deep traps assembled with point defect displacement damage by the γ-rays. By sharp contrast, the Ni/SiC diodes show a much larger decrease in forward current density for the same dose conditions. Since the changes in the SiC itself will be the same in each case, it is clear that the Ni contact is the cause of the larger changes. The on-state resistance can also be written

$$R_{on} = \frac{4V_B^2}{\mu\varepsilon E_c^2} + \rho_{sub}W_{sub} + R_C$$

where ρ_{sub}/W_{sub} are the resistivity/thickness of the SiC substrate and R_C is the contact resistance. Since the reverse characteristics show that V_B and ρ_{sub} show relatively small changes after irradiation, the decrease in forward current density is predominantly a result of the contact resistance term.

Figure 4-10 shows optical micrographs of the Ni(top) and WSi(bottom) contacts before and after Co-60 γ-irradiation to a dose of 315Mrad. While the latter show

negligible change in appearance, the Ni metallization shows a big change. This did not occur in the Ni ohmic contact on the backside of the rectifiers that had been annealed to minimize contact resistance. Preliminary Auger Electron Spectroscopy data indicated Ni rectifying contacts, which suggests reaction of the Ni with the SiC through a reaction of the type $2Ni+SiC \rightarrow Ni_2Si+C$. In the absence of radiation, this reaction does not occur until >600°C[Ip03, Mor00]. During the irradiation process, the temperature of the Ni was always <80°C. The reaction of the Ni with the underlying SiC is expected to reduce the effective electrical contact area, which would reduce the forward current density.

Table 4-4 summarizes the electrical properties of the Ni/SiC and WSi_X/SiC rectifiers before and after irradiation. The ideality factors and barrier heights of the WSi/SiC rectifiers were hardly affected by the γ-irradiation, whereas the ideality factor of the Ni/SiC devices was severely degraded and show an unphysical value after 315Mrad. The power figure-of-merit, V_B^2/R_{on}, are much more degraded for the Ni/SiC rectifiers for the same γ-ray dose, due to the increase in R_{on}.

WSi on GaN	ϕ_B(eV)	ϕ_F(eV)
As-deposited	0.49	0.37
400°C anneal	X	X
500°C anneal	X	X
600°C anneal	0.52	0.40
700°C anneal	0.50	0.39

Table 4-1 Barrier heights of WSi_X/GaN contacts as a function of anneal temperature.

Contact	Barrier Height(eV)	Ideality Factor
WSi (As-deposited)	0.97	2.1
WSi (500°C, 1 min, N_2)	1.2	1.2
WSi (700°C, 1 min, N_2)	0.99	1.1
WSi (900°C, 1 min, N_2)	0.69	1.2
WSi (1100°C, 1 min, N_2)	0.41	2.2
Ni (as-deposited)	1.1	1.7

Table 4-2 Summary of electrical data for annealed contacts.

WSi contacts	Barrier Height(eV)	Ideality Factor
25°C	1.2	1.1
100°C	1.3	1.1
200°C	1.4	1.1
300°C	1.5	1.1

Ni contacts	Barrier Height(eV)	Ideality Factor
25°C	1.0	1.7
100°C	1.2	1.4
200°C	1.3	1.3
300°C	1.4	1.3

Table 4-3 Summary of electrical data as a function of measurement temperature

	Barrier Height(eV)	Ideality Factor	V_B^2/R_{on}(kW/cm^2)
WSi(control)	1.17	1.1	4560
WSi(150Mrad)	1.04	1.1	3819
WSi(315Mrad)	1.26	1.1	2278
Ni(control)	0.95	1.7	3875
Ni(315Mrad)	0.91	6.2	60

Table 4-4 Characteristics of SiC Rectifiers before and after Co-60 γ-ray irradiations

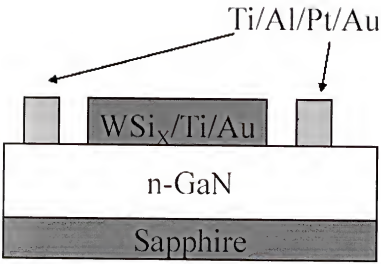

Figure 4-1 Schematic of WSiX/n-GaN Schottky diode

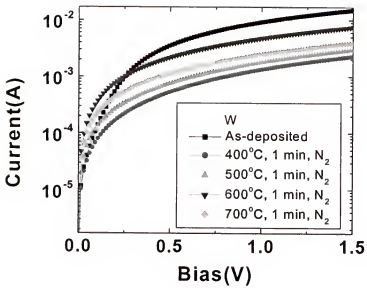

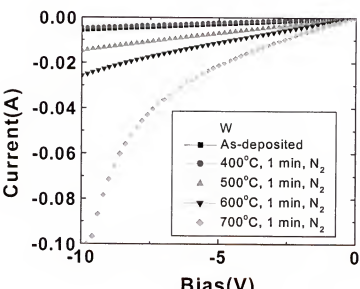

Figure 4-2 Forward(top) and reverse(bottom) I-V characteristics from W/GaN diodes as a function of anneal temperature

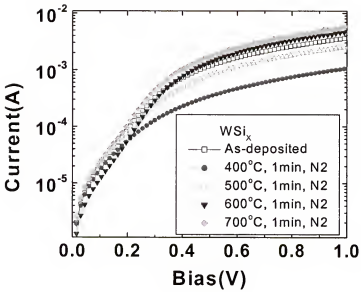

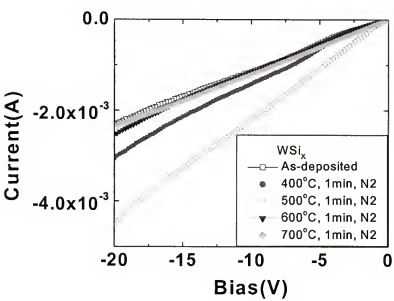

Figure 4-3 Forward(top) and reverse(bottom) I-V characteristics from WSiX/GaN diodes as a function of anneal temperature

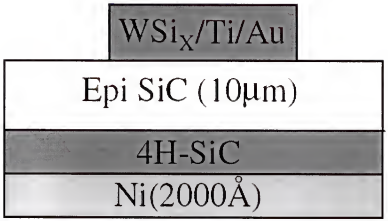

Figure 4-4 Schematic of WSi$_X$/SiC Schottky Diode.

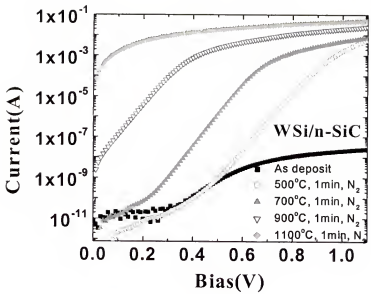

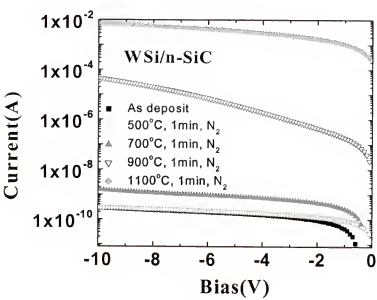

Figure 4-5 Forward(top) and reverse(bottom) I-V characteristics from WSiX diodes on 4H-SiC as a function of post-depositon annealing temperature.

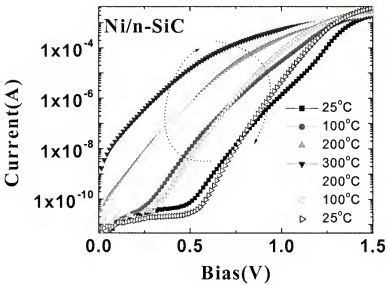

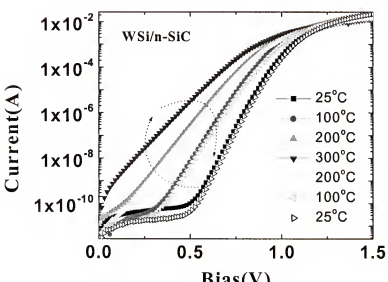

Figure 4-6 Forward I-V characteristics from Ni(top) and WSi_X(bottom) diodes on 4H-SiC as a function of measurement temperature. The WSi_X contacts were annealed at 500°C for 1min after deposition.

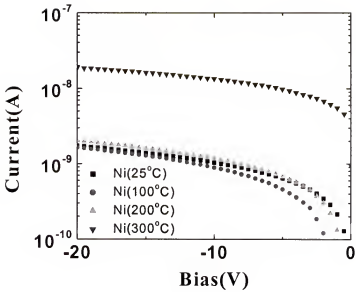

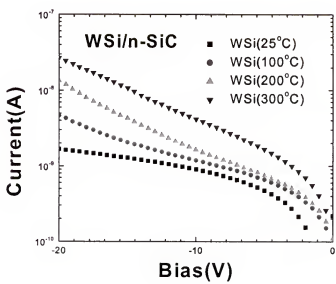

Figure 4-7 Reverse I-V characteristics from Ni(top) and WSi(bottom) diodes on 4H-SiC as a function of measuremental temperature. The WSi_X contacts were annealed at 500°C for 1 min after deposition

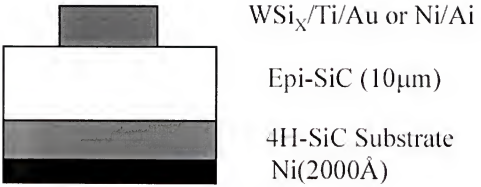

Figure 4-8 Schematic of SiC Schottky rectifiers.

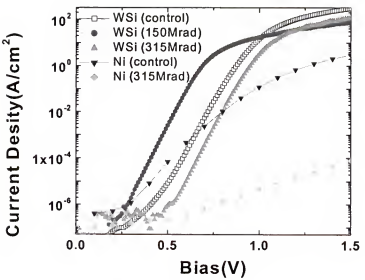

Figure 4-9 Forward I-V characteristics of WSiX/SiC and Ni/SiC rectifiers before and after Co-60 γ-irradiation to doses up to 315Mrad

(top)

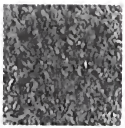

Ni(control, 315Mrad)

(bottom)

WSi(control, 315Mrad)

Figure 4-10 Optical micrographs of Ni(top) and WSiX/Ti/Au(bottom) contacts before and after Co-60 γ-irradiation to a dose of 315Mrad. The width of each micrograph is 40μm

CHAPTER 5
WIDE BANDGAP GAS SENSORS

5.1 Introduction

There is a strong interest in solid-state gas sensors for applications including fuel leak detection in automobiles and aircraft, fire detectors, exhaust diagnosis and emissions from industrial processes.[Arb93, Bar95, Che96, Che98, Con02, Eke98, Hun01, Hun02, Sav00, Spe00, Spe97, Sve99, Tob97, Vas98] SiC is capable of operating at much higher temperatures than more conventional semiconductors such as Si because of its large bandgap(3.26eV for the 4H-SiC polytype vs 1.1eV for Si).[Cas98] Simple Schottky diode or field-effect transistor structure fabricated in SiC are sensitive to a number of gases, including hydrogen and hydrocarbons.[Hun02, Spe97] The sensing mechanism is thought to be creation of a polarized layer on the semiconductor surface by hydrogen atoms diffusing through the metal contact.[Bar95]

There is also great interest in developing GaN based wide bandgap semiconductor sensors due to their potential for high temperature operation and the ability to integrate them with power or microwave electrodes or with UV solar-blind detectors and emitters fabricated in the same materials. There have been a number of reports on the gas-sensing properties of GaN Schottky diodes[Lut99, Neu01b, Sch01, Sch02], but no comparisons of how different metals perform and little information in the temperature dependence of the time response.

5.2 Device Processing

5.2.1 4H-SiC Gas Sensors

Gas sensor were fabricated on 10μm of undoped($n\sim2\times10^{15}cm^{-3}$) grown on n^+($n\sim10^{19}cm^{-3}$) 4H-SiC substrates by vapor phase epitaxy. A full-area back-side e-beam evaporated Ni(2000Å)ohmic contact was annealed at 970°C for 3 mins to produce a low resistance ($1.5\times10^{-6}\,\Omega cm^2$) contact. The front-side rectifying contact of e-beam evaporated Pt(150Å thick) was patterned by lift-off. The diameter of Schottky contact was fixed at 80 μm, although much larger devices were also fabricated ($0.5 \times 0.5\ cm^2$). The devices were wire-bonded to a test fixture using Ti/Au bond-pads and Au wires. A schematic of the final device structure is shown in Figure 5-1. The gas sensing experiments were performed in a tube-furnace that contained electrical feed-throughs connected to either an HP4145 parameter analyzer or an I-V measurement system. Measurements were performed at either 25 or 150°C, with flowing gas ambients of N_2, 10%H_2 in N_2,air or CF_4.

5.2.2 GaN Gas Sensors

The sensors were fabricated on 6μm thick n-GaN($n\sim3\times10^{17}\ cm^{-3}$) layers grown on Al_2O_3 substrates by Metal Organic Chemical Vapor Deposition. Front-side ohmic contacts of Ti/Al/Pt/Au were formed by lift-off and subsequent annealing at 600°C. The Schottky contacts were formed by lift-off of e-beam deposited 24 nm of Pd or 15 nm of Pt. The devices were wire-bonded to a test fixture using Ti/Au bond-pads and Au wires for contact. Figure 5-6 shows a photograph of a completed device. The gas-sensing

experiments were carried out in a system described elsewhere[Kim03a], over a range of temperatures(25~200°C) with either N_2 or 10% H_2 in N_2 ambient.

5.3 Characteristics of SiC and GaN Based Gas Sensors

5.3.1 Characteristics of Pt/4H-SiC Gas Sensors

Figure 5-2 shows the forward I-V characteristics of the Pt/SiC diode at 25°C in pure N_2 and 10%H_2 in N_2 ambients. An advantage of these diodes is that they can be operated to large forward conduction currents, allowing very large signal differences resulting from different gas ambients. Note that the addition of 10% H_2 to the ambient produces a shift of 1.34V at a forward current of 0.2A. At lower voltage and current, the signal change was also easily discernable, eg. 47mA at a fixed forward bias of 1.5V or equivalently, 67mV at a fixed current of 6mA. The relative changes in reverse current were much smaller, with typical magnitudes of a few μA at –50V bias.

The SiC devices were also able to differentiate between various gases, as shown in Figure 5-3. The use of either air or CF_4 as the ambient produced significant increase in forward current. Since the H_2, O_2 and F_2 in these gases can affect the dipole layer at the Pt-SiC interface because of their reactivity, the electric field under the Pt gate is altered and produces the resulting change in diode forward current.

The diodes were operated up to 150°C for extended periods without deterioration of the Pt contact, although this is a significant concern for higher temperatures due to the possibility of $PtSi_2$ formation. For very high operating temperatures, it is desirable to use either a metal-oxide-semiconductor(MOS) approach[Spe00] or else employ more

thermally stable metallization such as W or WSi_x. Figure 5-4 shows the forward I-V characteristics in N_2 or 10%H_2 in N_2 ambients at both 25 and 150°C. The change in forward current upon changing the gas became larger at higher temperatures due to the increased dissociation efficiency of the gas molecules. The dissociation can occur through a catalytic reaction with the Pt gate, or through additional surface reactions on the semiconductor.[Spe00]

Figure 5-5 shows the time response of a SiC diode at 150°C upon switching the gas introduced into the enclosure from N_2 to 10%H_2 in N_2. Note that the change in voltage required to maintain a forward current of 30mA is very rapid(<1sec), with a saturation occurring ~4sec after the switch of the gases. The diffusion of hydrogen through the Pt layer is not the limiting factor in the time response of the diodes, but rather the mass transport of gas into the enclosure as observed by altering the introduction rate. Similarly, the initial recovery of the characteristics after introduction of the initial N_2 ambient is most likely dominated by removal of hydrogen atoms from the Pt/SiC interface or SiC interface. These results demonstrate the ability of SiC diodes to perform as rapid, sensitive gas sensors over a broad range of temperature.

5.3.2 Hydrogen-Sensitive GaN Schottky Diodes

Figure 5-7 shows the time response of Pt/GaN diodes to switching from N_2 to 10% H_2 in N_2 and back again, at a measurement temperature of 110°C with the diode biased at 1.5V forward bias. Note the rapid change in forward current as the H_2 is introduced and the shower decay back towards the original current level upon switching back to N_2. The barrier height, ϕ_B is given by

$\phi_B=\phi_m-\chi_S = eV_{BI}+\delta$

where ϕ_m is the metal workfunction, χ_S the electron affinity of GaN, e is the electronic charge, δ is the Fermi energy below the conduction band and V_{BI} is the build-in voltage. From the forward I-V characteristics, the barrier height($\Delta\phi_B$) was 50mV at 25°C and 70mV at 150°C for Pt/GaN diodes upon exposure to the 10% H_2 in N_2 ambient. The lowering of the barrier due to accumulation of hydrogen at the Pt/GaN interface is consistent with the formation of the dipole layers at the interface, as suggested previously[Sch02].

Figure 5-8 shows the response of a Pt/GaN diode to repeated cycling of the ambient from N_2 to 10% H_2 in N_2, with the sample held at 100°C. Even at this relatively modest temperature, the change in forward current for a fixed bias of 1.5V is readily detectable and shows there is sufficient cracking of the H_2 for the diode to be a sensitive gas detector. Note also that there is highly reproducible saturation current for each of the gas ambient employed.

The temperature dependence of the decay in forward current of 1.5V for Pt/GaN diodes is shown in Figure 5-9. The size of the change in current, and hence the change in ϕ_B, depends on temperature since cracking of the gas is more effective at higher temperatures. To gain some idea of the rate-determining mechanisms that are operative, the change in forward current at a fixed time of 50 seconds after switching of the gas was taken and plotted this change in Arrhenius form(Figure 5-10).

There are several features apparent in this data-firstly, the Pt/GaN diodes has a higher signal response than comparable Pd/GaN diodes. This is ascribed to the greater catalytic cracking efficiency of Pt for H_2. Secondly, the data does not show a single slope,

ie, there are multiple mechanisms at work. At high temperatures(≥110°C), the activation energy is of order 0.70eV. This is consistent with the activation energy for diffusion of hydrogen in materials such as metals[Pea91]. This suggests that the time needed for the atomic hydrogen to diffuse through the Pt to the interface with the GaN is the rate-limiting step under these conditions. As the temperature is lowered below 100°C, there are obviously other mechanism at work and it is plausible that under these conditions the initial dissociation of the H_2 is one of the rate-limiting steps, along with competing processes such as recombination of atomic hydrogen to form H_2 molecules.

Figure 5-11 shows forward I-V characteristics for Pd/GaN diodes at 170°C(top) or 200°C(bottom) in either N_2 or 10% H_2 in N_2 ambients. The changes in forward current upon introducing the H_2 are smaller than achieved with Pt/GaN diodes under the same conditions, as discussed above, but are still of sufficient magnitude to be useful as gas detectors at moderate temperatures. The choice of metallization may be dictated by the required operating temperature for the gas sensors. For example it may be necessary to use W-based schemes[Pea99] or carbides that have extremely high thermal stability if operating temperatures above 400°C are required.

The change in forward current for Pd/GaN diodes at two different temperatures are shown in Figure 5-12 for cycling between N_2 and 10% H_2 in N_2. The forward current density J can be expressed as

$$J = J_0 \exp(\frac{eV}{kT})$$

where k is Boltzman's constant, T is the absolute measurement temperature and J_0 is dependent on ϕ_B. From the forward I-V characteristics, a change in barrier height of

30mV at 150°C and 60mV at 200°C upon introduction of H_2 into the ambient for the Pd diodes were found.

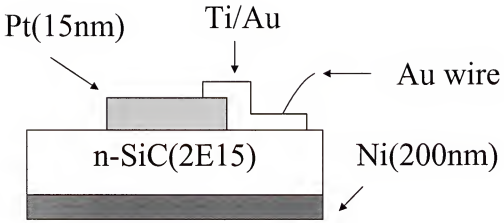

Figure 5-1 Schematic of Pt/4H-SiC gas sensor.

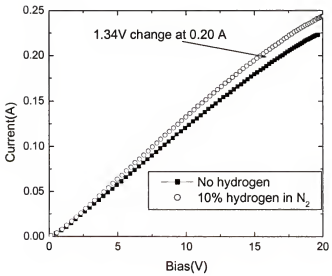

Figure 5-2 High forward bias I-V characteristic from SiC sensor in pure N_2 or 10%H_2 in N_2 ambients at 25°C.(80μm diameter)

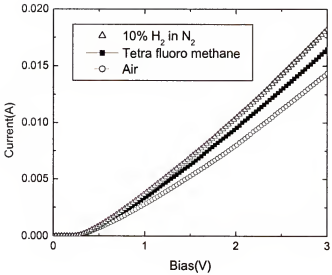

Figure 5-3 Log forward bias I-V characteristics from SiC sensor in 10%H2 in N2, pure N2 or CF4 ambients at 25°C. (80μm diameter).

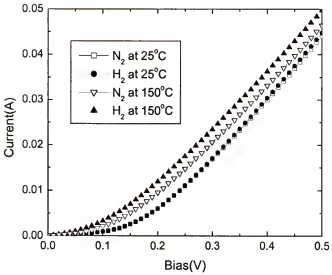

Figure 5-4 Low bias forward I-V characteristics from SiC sensor in 10%H_2 in N_2 or pure N_2 ambients at the different temperatures.(Size of contact is 0.5cm×0.5cm).

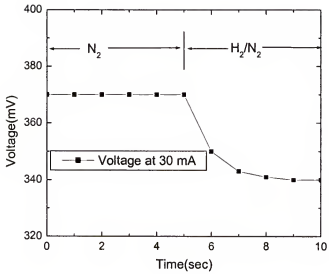

Figure 5-5 Time response of SiC sensor upon changing from pure N_2 to 10%H_2 in N_2 ambient at 150°C. The y-axis shows the forward bias required to maintain a current of 30mA.

Figure 5-6 Photograph of completed Pt/n-GaN diode

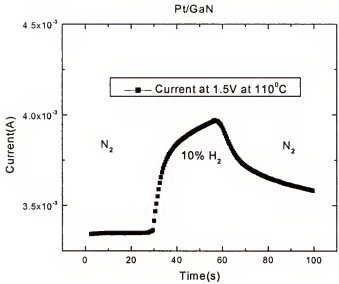

Figure 5-7 Time response at 110°C of forward current of a Pt/GaN diode forward biased at 1.5V, upon switching from N_2 ambient to 10% H_2 in N_2 and then back to N_2.

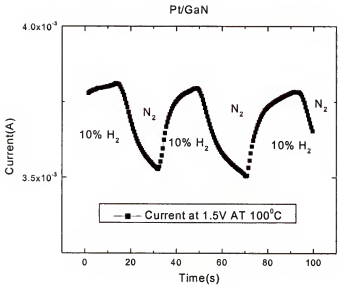

Figure 5-8 Time response at 100°C of forward current of a Pt/GaN diode biased at 1.5V, upon cycling the ambient between pure N_2 and 10% H_2 in N_2.

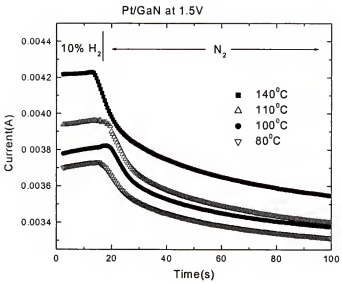

Figure 5-9 Decay of forward current as a function of measuremental temperature for Pt/GaN diodes at 1.5V forward bias after switching from 10% H_2 in N_2 ambient to pure N_2.

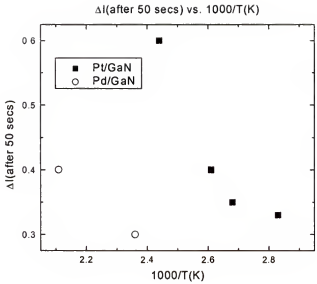

Figure 5-10 Arrhenius plot of change in forward current of Pt/GaN diodes 50 secs after switching from 10% H_2 in N_2 ambient to pure N_2.

Top

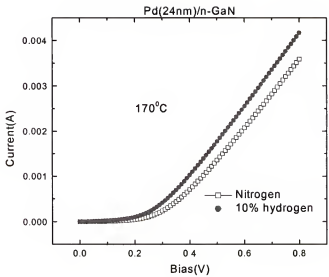

Bottom

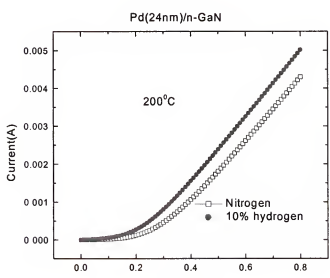

Figure 5-11 Forward I-V characteristics from Pd/GaN diodes measured in N_2 or 10% H_2 in N_2 ambient at either 170°C(top) or 200°C(bottom).

Top

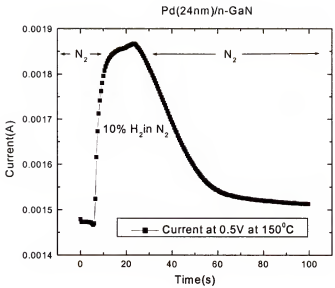

Bottom

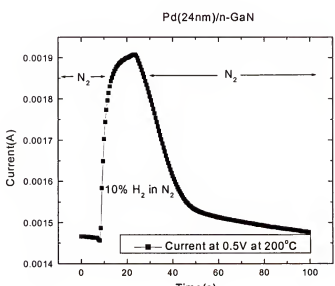

Figure 5-12 Forward current at 0.5V bias at 150°C(top) or 200°C(bottom) for Pd/GaN diodes cycled in N_2 and 10% H_2 in N_2 ambient.

CHAPTER 6
SUMMARY AND FUTURE WORK

6.1 GaN MOS Diodes

GaN metal oxide semiconductor diodes were demonstrated utilizing MgO as the gate oxide. An interface trap density of low-to-mid 10^{11} $eV^{-1}cm^{-2}$ was obtained from temperature conductance-voltage measurements. Terman method was also used to estimate the interface trap density and a slight lower number was obtained as compared to the conductance method. Results from elevated temperature (up to 300°C) conductance measurements showed an interface state density roughly three times higher(6×10^{11} eV^{-1} cm^{-2}) than at 25°C.

Future efforts should be the trap passivation. In Silicon industry, surface states can be minimized by annealing the samples in hydrogen ambient. Hydrogen species can attached to a dangling Si bond to make it inactive. In SiC MOSFET, NO and NH_3 are also used to passivate surface states. But it is still unknown what kind of gases can be used to passivate surface states in GaN.

6.2 MgO/GaN Gate-controlled Diodes

Gate-controlled n^+p metal-semiconductor-oxide(MOS) diodes were fabricated in p-GaN using MgO as a gate dielectric and Si^+ implantation to create the n^+ regions. This structure overcomes the low minority carrier generation rate in GaN and allowed observation of clear inversion behavior in the dark at room temperature. By contrast,

diodes without the n^+ regions to act as an external source of minority carriers did not show inversion even at measurement temperatures of 300ºC. The gated diodes showed the expected shape of the current-voltage characteristics, with clear regions corresponding to depletion and inversion under the gate. The MgO was deposited prior to the Si implantation and was stable during the activation annealing for the Si-implanted n^+ regions. Despite remarkable recent progress in depletion-mode AlGaN/GaN HEMTs, there were not many reports about enhancement-mode devices[Moo02] in III-nitride. More than 25 years of intensive research was necessary to demonstrate the first enhancement mode GaAs-MOSFET[Ren96a], and enhancement-mode InGaAs-MOSFET[Ren97] using a mixture of gallium oxide(Ga_2O_3) and gadolinium oxide(Gd_2O_3) as gate dielectric material. The initial demonstration of enhancement-mode GaN MOSFET was reported[Iro04], but still there is room for improvements.

6.3 Inversion Behavior in Sc_2O_3/GaN Gate-controlled Diodes

The capacitance-voltage(C-V) characteristics of Sc_2O_3/p-GaN gate-controlled diodes show unusual hook shapes due to the charging of surface states. From the drain-voltage dependence of the C-V curves, the total surface state density was estimated to be ~ 8.2×10^{12} cm^{-2} for diodes undergoing an implant activation anneal at 950°C. The accumulation capacitance showed a significant dependence on measurement frequency and is suggested to result from the presence of an interfacial dielectric between the Sc_2O_3 and GaN. The Si-implanted n^+ regions in the gated diode structure are effective in providing a source of inversion charge. Recent report shows the activation efficiency reaches a maximum of 30% after annealing at 1200°C for 2 min[Iro03]. Activation

temperature and annealing time should be optimized to minimize the nitrogen vacancy and maximize the activation efficiency.

6.4 Thermal Stability of WSi_X and W Metallization on GaN

WSi_X Schottky contacts on GaN are found to exhibit improved thermal stability compared to pure W contacts. While the W contacts degrade for anneal temperatures ≥500°C through reaction with the GaN to form β-W_2N, the WSi_X contacts show a stable Schottky barrier height of ~0.5eV as obtained from current-voltage(I-V) measurements. The reverse leakage current in both types of diodes is considerably higher than predicted from thermionic emission. The reverse current density was found to vary approximately as $V_B^{0.5}$ (V_B is the reverse bias) and suggests the presence of additional current transport mechanism in both types of diodes. WSi_X was successfully used as self-aligned mask in GaAs, but the activation temperature is higher in GaN, it seems that WSi_X cannot satisfy the procedure. To find right material for self-aligned process, other refractory metals also can be investigated.

6.5 Thermal Stability of WSi_X Schottky Contacts on 4H-SiC

Sputter-deposited $WSi_{0.45}$ rectifying contacts were characterized on n-type 4H-SiC as a function of annealing and measurement temperature. The as-deposited contacts show evidence of recombination-dominated carrier transport and a high series resistance due to ion-induced damage occurring during the Ar plasma-assisted deposition. Annealing at 500°C for 1min produces a maximum barrier height of 1.15eV and reduces the diode ideality factor. The contacts are degraded by annealing at >700°C but show reduced

forward and reverse currents when measured at elevated temperature(300°C) compared to the more common Ni rectifying contacts. To demonstrate the self-aligned process in SiC, other refractory metal system can be investigated.

6.6 High Dose Gamma-ray Irradiation on Rectifiers

SiC Schottky rectifiers with either WSi_X or Ni rectifying contacts were irradiated with Co-60 γ-rays to doses up to ~315Mrad. The Ni/SiC rectifiers show severe reaction of the contact at the highest dose, badly degrading the forward current characteristics and reducing the power figure-of-merit V_B^2/R_{on} (where V_B is the reverse breakdown voltage and R_{on} is the on-state resistance) from 3.88 MW/cm^2 in the control diodes to 60kW/cm^2 after irradiation. By sharp contrast, the WSi_X/SiC devices show little deterioration of the contact with the same conditions and the power figure-of-merit is reduced by only a factor of ~2 upon irradiation. For application in space-shuttle, and satellite communication system, these refractory metals have a lot of potentials.

6.7 Characteristics of SiC Gas Sensors

Pt/4H-SiC Schottky diode rectifiers show rapid(<1 sec) changes in forward current upon introduction of different gases(N_2, air, H_2, CF_4) into the ambient. The diodes can be operated at large forward currents, leading to large signal sizes for switching from one gas ambient to another. A shift of 1.34V at 25°C was obtained at a fixed forward current of 0.2A for switching from N_2 to 10% H_2 in N_2. The signal size increases with increasing measurement temperature due to more efficient cracking of the gas molecules. To maximize the signal change, the device structure and the thickness of catalytic metals can

be optimized, also other refractory metals can be used as diffusion barrier to increase the high temperature stability.

6.8 GaN Hydrogen Sensors

Pt/n-GaN and Pd/n-GaN Schottky diodes were characterized for their response to hydrogen as a function of measurement temperature. Even at modest temperatures(80~140°C), an 80μm diameter diode shows a large increase(≥0.5mA) in forward current upon introduction of ~10% H_2 into a N_2 ambient. The change in current increases with measurement temperature and begins essentially immediately upon introduction of the hydrogen. Cycling the ambient from N_2 to 10%H_2 in N_2 and back to N_2 produces reproducible cycling of the forward current at fixed forward bias. The decrease in barrier height of Pt on GaN was 50mV at 25°C and 70mV at 150°C upon introduction of H_2 into the ambient,with lower values for Pd. At high temperature, the time response of the sensors appears to be controlled by hydrogen diffusion to the metal/GaN interface, while at low temperatures(<100°C), dissociation of the gas appears to be the rate-determining step.

To increase selectivity, the large array using different sensitive coating can be used to identify specific species. In addition, integrated with Power amplifier such as Microwave Monolithic Integrated Circuit(MMIC), these devices can operate as remote sensors.

LIST OF REFERENCES

Aka91 Akasaki, I., H. Amano, M. Kiti, and K. Hiramatsu, J. Lumin. 48/49, 666(1991).

Ale01 Alexandrov, P., J. H. Zhao, W. Wright, M. Pan, M. Weiner, Electron. Lett. 37, 1261(2001).

Ale98 Alexe, M., Appl. Phys. Lett. 72(18), 2283(1998).

Ale99 Alekseev, E., A. Eisenbach, D. Pavlidis, Electron. Lett. 35, 24(1999).

Alo97 Alok, D. and B.J. Baliga, IEEE Electron. Dev. Lett. 44, 1013 (1997).

Amo98 Amano, H., Appl. Phys. Lett. 48, 352(1986).

Arb93 Arbab, A., A. Spetz and I. Lundström, Sens. Actuators B 15/16, 19(1993).

Aru98 Arulkumaran, S., T. Egawa, H. Ishikawa, T. Jimbo, and M. Umeno, Appl. Phys. Lett. 73, 809(1998)

Bar95 Baranzahi, A., A. Lloyd Spetz and I. Lundström, Appl. Phys. Lett. 67, 3203(1995).

Ber66 Berglund, C. N., IEEE Trans. Elect. Dev., 13, 701(1966).

Bin01 Binari, S. C., K. Ikossi, J. A. Roussos, W. Kruppa, D. Park; H. B. Dietrich, D. D. Koleske, A. E. Wickenden, and R. L. Henry, IEEE Trans. Electron Dev. 48, 465(2001).

Bin97a Binari, S. C., W. Kruppa, H. B. Dietrich, G. Kelner, A. E. Wickenden and J. A. Freitas Jr., Sol.-State Electron. 41, 1549(1997).

Bin97b Binari, S. C., K. Doverspike, G. Kelner, H. B. Dietrich and A. E. Wickenden, Sol.-State Electron. 41, 177(1997)

Bla63 Black, J., H. Lowckwood, and S. Mayburg, J. Appl. Phys. 34, 178(1963).

Cas00 Casady, J.B., in Processing of Wide Bandgap Semiconductor (William Andrew, Norwich, NY, 2000).

Cas71 Castagne, R and A. Vapaille, Sufe. Sci., 28, 157(1971).

Cas96a Casey, H. C., Jr., G. G. Fountain, R. G. Alley, B. P. Keller, S. P. DenBaars, Appl. Phys. Lett. 68, 1850(1996).

Cas96b Casady, J. B. and R. W. Johnson, Sol.-State Electron. 39, 1409(1996).

Cas98 Casady, J. B., A. K. Agarwal, S. Seshadri, R. R. Siergiej, L. B. Rowland, M. F. MacMillan, D. C. Sheridan, P. A. Sanger and C. D. Brandt, Sol.-State Electron. 42, 2165(1998).

Cas98 Casady, J. B., A. K. Agarwal, S. Seshadri, R. R. Siergiej, L. B. Rowland, M. F. MacMillan, D. C. Sheridan, P. A. Sanger and C. D. Brandt, Sol.-State Electron. 42, 2165(1998).

Che01 Chen, P., W. Wang, S. J. Chua, and Y. D. Zheng, Appl. Phys. Lett. 79, 3530(2001).

Che02 Chen, T., Z. Luo, J. D. Cressler, T. F. Isaacs-Smith, J. R. Williams, G. Y. Chung and S. D. Clark, Sol.-state Electron. 46, 2231(2002).

Che96 Chen, L. Y., G. W. Hunter, P. G. Neudeck, D. L. Knight, C. C. Liu, and Q. H. Wu, Proceeding of the Third International Symposium on Ceramic Sensors, H. U. Anderson, M. Liu, and N. Yamazoe, Editors, Electro. Soc. Inc. Pennington, NJ, 92(1996).

Che97 Chen, L., G. W. Hunter, and P. G. Neudeck, J. Vac. Sci. Technol A 15, 1228(1997).

Che98 Chen, L., G. W. Hunter, and P. G. Neudeck, J. Vac. Sci. Techonol. A16, 2890(1998).

Col00 Cole, M. W., P. C. Joshi, C. W. Hubbard, M. C. Wood, M. H. Ervin, B. Geil, and F. Ren, J. Appl. Phys. 88, 2652(2000).

Col02 Cole, M. W., C. W. Haffard, J. D.Demaree,J.K.Hirvonen,M.H.Ervin and M. C. Wood, Army Research Conference, Orlando(2002).

Col96 Cole, M. W., D. W. Eckart, W. Y. Han, R. L. Pfeffer, T. Monahan, F. Ren, C. Yuan, R. A. Stall, S. J. Pearton, Y. Li, and Y. Lu, J. Appl. Phys. 80, 278(1996).

Col97 Cole, M. W., F. Ren, S. J. Pearton, J. Electrochem. Soc. 144, L275(1997).

Con02 Connolly, E. J., G. M. O'Halloran, H. T. M. Pham, P. M. Sarro and P. J. French, Sens. Actuators A99, 25(2002)

Cro97 Crofton, J., L.M. Porter, and J.R. Williams, Phys. Stat. Solidi B202, 581(1997)

Dau99 Daumiller, T., C. Kirchner, M. Kamp, K. J. Ebeling, and E. Kohn, IEEE Electron. Dev. Lett. 20, 448(1999)

Eas01 Eastman, L. F., V. Tilak, J. Smart, B. M. Green, E. M. Chumbes, R. Dimitrov, H. Kim, O. S. Ambacher, N. Weimann, T. Prunty, M. Murphy, W. J. Schaff, and J. R. Shealy, IEEE Trans. Electron Dev., 48, 479(2001)

Eke98 Ekedahl, L.-G., M. Eriksson and I. Lundstrom, Acc. Chem. Res 31, 249(1998).

Fu02 Fu, D. J., Y. H. Kwon, T. W. Kang, C. J. Park, K. H. Baek, H. Y. Cho, D. H. Shin, C. H. Lee, and K. S. Chung, Appl. Phys. Lett. 80, 446(2002)

Gaf01 Gaffey, L. J. Guido, X. W. Wang, and T. P. Ma, IEEE Trans. Electron Dev. ED48, 458(2001)

Gil01 Gila, B. P., J. W. Johnson, R. Mehandru, B. Luo, A.H. Onstine, K. K. Allums, V. Krishnamoorthy, S. Bates, C. R. Abernathy, F. Ren and S. J. Pearton, Phys. Stat. Solidi A 188, 239-253(2001).

Goe68 Goetzberger, A., and J. C. Irvin, IEEE Trans. Electron Dev. ED-15, 1005(1968)

Gre00 Green, B. M., K. K. Chu, E. M. Chumbes, J. A. Smart, J. R. Shealy, and L. F. Eastman, IEEE Electron. Dev. Lett., 21, 268(2000)

Gro66 Grove, S. and D. J. Fitzgerald, Sol.-State Electron. 9, 783(1966).

Has00 Hashizume, T., E. Alekseev, D. Pavlidis, K. S. Boutros, and J. Redwing, J. Appl. Phys. 88, 1983(2000).

Hon00a Hong, M., H. Ng, M. Kwo, A. Kortran, A. Y. Cho, F. Ren, J.-I. Chyi, C. R Abernathy and S. J. Pearton, Mat. Res. Soc. Symp. 622, T2.2(2000).

Hon00b Hong, M., K. A. Anselm, J. Kwo, H. M. Ng, J. N. Baillargeon, A. R. Kortan, J. P. Mannaerts, A. Y. Cho, C. M. Lee, J. I. Chyi, and T. S. Lay , J. Vac. Sci. Technol. B. 18, 1453(2000).

Hon00c Hong, M., H.M. Ng, J. Kwo, A.R. Kortan, J.N. Baillargeon, S.N.G. Chu, J.P. Mannaerts, A.Y. Cho, F. Ren, C.R. Abernathy, S.J. Pearton, presented at 197th Electrochem. Soc. Meeting, May 2000, Toronto, ON, Canada.

Hu01 Hu, X., A. Koudymov, G. Simin, J. Yang, M. A. Khan, A. Tarakji, M. S. Shur and R. Gaska, Appl.Phys.Lett.79, 2832(2001).

Hun01 Hunter, G. W., C.C. Liu, D. Makel, MEMS *Handbook*, ed. M. G. Hak (CRC Press, Boca Raton, (2001).

Hun02 Hunter, G. W., P. G. Neudeck, R. S. Okojie, G. M. Beheim, V. Thomas, L. Chen, D. Lukco, C. C. Liu, B. Ward and D. Makel, Proc. ECS Vol 01-02, 212(2002)

Ip03 Ip, K., Nigam, K. H. Baik, F. Ren, G. Y. Chung, B. P. Gila, and S. J. Pearton, J. Electrochem. Soc. 150, 6293(2003).

Iro03 Irokawa, Y., J. Kim, F. Ren, K. H. Baik, B. P. Gila, C. R. Abernathy, S. J. Pearton, C.-C. Pan, G.-T. Chen, and J.-I. Chyi, Appl. Phys. Lett., 83, 4987(2003)

Iro04 Irokawa, Y., Y. Nakano, M. Ishiko, T. Kachi, J. Kim, F. Ren, B. P. Gila, A. H. Onstine, C. R. Abernathy, S. J. Pearton, C. -C. Pan, G. -T. Chen, and J. -I. Chyi(In press)

Ito79 Ito, K., Surf. Sci. 86, 345(1979).

Ito97 Itoh, A., H. Matsunami, Phys. Stat. Solidi A162, 389(1997)

Iva01 Ivanov, P.A., M. E. Levinshtein, G. Simin, X. Hu, J. Yang, M. A. Khan, S. C. Rumyantsev, M. S. Shur and R. Gaska, Electron. Lett. 37, 1479(2001)

Jia03 Jiang, J., O. Awadelkarim, D. -O Lee, P. Roman and J. Ruzyllo, Sol.-State Electron. (in press)

Joh00 Johnson, J. W., B. Luo, F. Ren, B. P. Gila, V. Krishnamoorthy, C. R. Abernathy, S. J. Pearton, J. I. Chyi, T. E. Nee, C. M. Lee, and C. C. Chuo, Appl. Phys. Lett. 77, 3230(2000).

Joh01 Johnson, J. W., B. P. Gila, B. Luo, K. P. Lee, C. R. Abernathy, S. J. Pearton, J. I. Chyi, T. E. Nee, C. M. Lee, C. C. Chou, and F. Ren, J. Electrochem. Soc. 146, G303(2001).

Joh02 Johnson, N. M., A. V. Nurmikko, and S. P. Denbaars, Phys. Today, 31(2000).

Kaw98 Kawai, H., M. Hara, F. Nakamura and S. Imanaga, Electron. Lett. 34, 592(1998)

Kes00 Kestle, A., S. P. Wilks, P. R. Dunstan, M. Pritchard, P. A. Mawby, Electron. Lett. 36, 267(2000).

Kha00 Khan, M. A., X. Hu, G. Simin, G. Lunev, J. Yang, R. Gaska, M. S. Shur, IEEE Electron Dev. Lett. 21, 63-65(2000).

Kha01 Khan, M. A., X. Hu, A. Tarakji, G. Simin, J. Yang, R. Gaska, and M. S. Shur, Appl. Phys. Lett. 77, 1339(2000).

Kik03 Kikkawa, T., M. Nagahara, N. Adachi, S. Yokokawa, S. Sato, M. Yokoyama, M. Kanamura, Y. Yamaguchi, N. Hara, and K. Joshin, IEEE Radio Freq. Inte. Cir. Sym., MO3C-5,167(2003)

Kim03a Kim, J., B. P. Gila, C. R. Abernathy, G. Y. Chung, F. Ren and S. J. Pearton, J. Electron. Mat.(in press)

Kim03b Kim, J., S. Nigam, F. Ren, D. Scheonfeld, G. Y. Chung, and S. J. Pearton, Electrochem. Sol.-State Lett. 6, G289(2003).

Kni02 Knights, A. P., M. A. Lourenço, K. P. Homewood, D. J. Morrison, N. G. Wright, S. Ortolland, C. M. Johnson, A. G. O'Neill, P. G. Coleman, K. P. Hilton, and M. J. Uren, J. Appl. Phys. 87, 3973(2002).

Koh99 Kohn, E., I. Daumiller, P. Schmid, N. X. Nguyen, C. N. Nguyen, Electron. Lett. 35, 1022(1999)

Lay01a Lay, T. S., M. Hong, T. Kwo, T. P.Lee, W. Hung and D. T. Huang, Sol.-State Electron. 45, 1679(2001).

Lay01b Lay, T. S., W. D. Liu, M. Hong, J. Kwo, and J. P. Mannasrts, Electron. Lett. 37(9), 595(2001)

Lee00 Lee, S.-K., C.-M. Zetterling, and M. Östling, J. Appl. Phys. 87, 8039(2000).

Lee01a Lee, J.-S., A. Vescan, A. Wieszt, R. Dietrich, H. Leier, Y.-S. Kwon, Electron. Lett. 37, 130(2001).

Lee01b Lee, S.-K., C.-M. Zetterling, and M. Ostling, J. Electron. Mater. 30, 242(2001).

Lee02 Lee, K. W, D. W. Chou, H. R. Wu, J. J. Huang, Y. H. Wang, M. P Hound, S. J. Chang, and Y. K. Su, Elec. Lett., 38, 829(2002).

Lu01 Lu, W., J. Yang, M. A. Khan and I. Adesida, IEEE Trans. Electron Dev., ED48, 581(2001)

Luc01 Luckowski, E.D.,J.M.DeLucca,J.R.Willimas,S.E.Mohney,M.J.Bozack,T.Isaacs-Smith and J.Crofton, J. Electron. Mater. 27, 330(2001).

Lun00 Lundberg, N., M. Östling, C.-M. Zetterling, P. Tägtström, and U. Jansson, J. Electron. Mater. 29, 372(2000).

Lun75 Lundström, I., M. S. Shivaraman, and C. M. Svensson, J. Appl. Phys., 46, 3876(1975).

Lun76 Lundström, I., M. S. Shivaraman, L. Stiblert, and C. Svensson, Rev. Sci. Instrum. 47, 738 (1976)

Lun96 Lundberg, N., S. -K. Lee and M. Ostling, J. Electrochem. Soc. 143, 662(1996)

Luo02 Luo, B., J. W. Johnson, J. Kim, R. M. Mehandru, F. Ren, B. P. Gila, A. H. Onstine, C. R. Abernathy, S. J. Pearton, A. G. Baca, R. D. Briggs, R. J. Shul, C. Monier, and J. Han, Appl. Phys. Lett. 80, 1661(2002).

Lut99 Luther, B. P., S. D. Wolter, S. E. Mohney, Sens. Actuators B56, 164(1999).

Mel97 Melloch, M. R. and J. A. Cooper, Jr., MRS Bulletin 22, 42(1997).

Mok98 Mok, D., R. Egloff and E. Arnold, Mat. Sci. Forum 264, 929(1998).

Moo02 Moon, J. S., D. Wong, T. Hussain, M. Micovic, P. Deelman, M. Hu, M. Antcliffe, C. Ngo, P. Hashitomo, and L. McCray, Device Research Conference Digests, 23(2002).

Mor00 Morrison, D. J., N. G. Wright, A. B. Horsfall, C. M. Johnson, A. G. O'Neill, A. P. Knights, K. P. Hilton and M. J. Uren, Sol.-State Electron. 44, 1879(2000).

Mor01 Morisette, D.T., J.A. Cooper, Jr., M.R. Melloch, G.A. Dolny, P.M. Shenoy, M. Zafrani, and J. Gladish, IEEE Trans. Electron. Dev. 48, 349 (2001).

Mor94 Morkoc, H., S. Strite, G. B. Gao, M. E. Lin, B. Sverdlov, and M. Burnd, J. Appl. Phys. 76, 1363(1994).

Nak94 Nakamura, S., T. Mukai, and M. Senoh, Appl. Phys. Lett. 64, 1687(1994).

Nak95 Nakamura, S., J. Vac. Sci. Technol., A13, 705 (1995).

Neu01a Neuberger, R., G. Muler, O. Ambacher, and M. Stutzmann, Phys. Stat. Solidi A 183, R10(2001)

Neu01b Neuberger, R., G. Muler, O. Ambacher, and M. Stutzmann, Phys. Stat. Solidi A185, 85(2001).

Ngu00 Nguyen, N. X., M. Micovic, W.-S. Wong, P. Hashimoto, L.-M. McCray, P. Janke, C. Nguyen, Electron. Lett. 36, 468(2000).

Ngu99 Nguyen, N. X., C. Nguyen and D. E. Grider, Electron. Lett. 35, 1356(1999).

Nic82 Nicollian, E. H. and J. R. Brews, MOS Physics and Technology, John Wiley, 1982

Nig02 Nigam, S., J. Kim, F. Ren, G. Y. Chung, M. F. MacMillan, R. Dwivedi, T. N. Fogarty, R. Wilkins, K. K. Allums, C. R. Abernathy, S. J. Pearton, and J. R. Williams, Appl. Phys. Lett. 81, 2385(2002).

Nig03 Nigam, S., J. Kim, F. Ren, G.Y. Chung, C.R. Abernathy, S.J. Pearton, Appl. Phys. Lett.(in press)

Ode98 Oder, T. N., J. R. Williams, M. J. Bozack, V. Iyer, S. E. Mohney and J. Crofton, J. Electron. Mater. 27, 324(1998).

Osk00 Oskam, G., P. C. Searson, and M. W. Cole, Appl. Phys. Lett., 76, 1300(2000).

Pea00 Pearton, S. J., F. Ren, A. P. Zhang and K. P. Lee, Mat. Sci. Eng. R 30, 55(2000)

Pea91 Pearton, S. J., J. W. Corbett, and Michael Stavola, Hydrogen in Crystalline Semiconductor(Springer-Verlag, Berlin 1991)

Pea99 Pearton, S. J., J. C. Zolper, R. J. Shul, F. Ren, J. Appl. Phys. 86,1(1999).

Pie96 Pierret, R. F, Semiconductor Device Fundamentals, Addison-Wesley(1996).

Pet97 Peters, D., R. Schoener, K.H. Holzein, and P. Friedrichs, Appl. Phys. Lett. 71, 2996 (1997).

Pon97 Fonce, F. A., and D. P. Bour, Nature, 386, 351(1997).

Por95 Porter, L. M. and R. F. Davis, Mat. Sci. Eng. B34, 83(1995)

Ren96a Ren, F., M. W. Hong, W. S. Hobson, J. M. Kuo, J. R. Lothian, J. P. Mannaerts, J. Kwo, Y. K. Chen, and A. Y. Cho, International Electron Device Meeting Digest, 943(1996).

Ren97 Ren, F., M. Hong, J. M Kwo, W. S. Hobson, H. S. Tsai, J. R. Lothian, J. P. Mannaerts, J. Kwo, S. N. G. Chu, J. Lin, Y. K. Chen, and A. Y. Cho, Device Research Conference Digest, 78(1997).

Ren98a Ren, F., C.R. Abernathy, J.D. MacKenzie, B.P. Gila, S.J. Pearton, M. Hong, M.A. Marcus, M.J. Schurman, A.G. Baca, R.J. Shul, Sol.-State Electron., 42, 2177 (1998).

Ren98b Ren, F., M. Hong, S.N.G. Chu, M.A. Marcus, M.J. Schurman, A. Baca, S.J. Pearton, C.R. Abernathy, Appl. Phys. Lett., 73, 3893 (1998).

Rut81 Ruths, P. F., S. Ashok, S. J. Foash and J. M. Ruths, IEEE Transaction on Electron. Dev. 28, 1003(1981).

Sah88 Sah, C. T., Proc. Of the IEEE, 1280(1988).

Sav00 Savage, S. M., A. Konstantinov, A. M. Saroukan and C. Harris, Proc. ICSCRM 1999 511(2000).

Sax99 Saxena, V., J.N. Su, and A.J. Steckl, IEEE Trans. Electron. Dev. 46, 456(1999).

Sch01 Schalwig, J., G. MulerO. Ambacher, and M. Stutzmann, Phys. Stat. Sol. A185, 39(2001).

Sch02 Schalwig J., G. Muler, M. Eickoff, O. Ambacher, and M. Stutzmann, Mat. Sci. Eng. B101, 86(2002).

Sch86 Schroder, D. K., Advanced MOS Diodes, Addison Wesley Longman, New York (1986).

Sch98a Schroder, D. K., Semiconductor Material and device Characterization, Wiley and sons, New York (1998)..

Sch98b Schoen, K. P., J. M. Woodall, J. A. Cooper, and M. R. Melloch, IEEE Trans. Electron. Dev. 45, 1595(1998).

She94 Sheppard, S. T., J. A. Cooper, Jr., and M. R. Melloch, J. Appl. Phys, 75, 3205(1994)

Shu98 Shur, M. S., Sol.-State Electron. 42, 2131(1998).

Sim00 Simin, G., X. Hu, N. Ilinskaya, A. Kumar, A. Koudymov, J. Zhang, M. Asif Khan, R. Gaska, M. S. Shur, Electron. Lett. 36, 2043(2000).

Sim01 Simin, G., X. Hu, N. Ilinskaya, J. Zhang, A. Tarakji, A. Kumar, J. Yang, M. Asif Khan, P. Gaska, M. S. Shur, IEEE Electron. Dev. Lett. 22, 53(2001).

Sin02a Singh, R., D. C. Capell, K . G. Irvine, J. T. Richmond, J. W. Palmour, Electron. Lett. 38, 1738(2002).

Sin02b Singh, R., J.A. Cooper, Jr., M.R. Melloch, T.P. Chow, and J.W. Palmour, IEEE Trans. Electron. Dev. 49, 6650(2002).

Skr00 Skromme, B.J., E. Luckowski, K. Moore, M. Bhatnagar, C.E. Weitzel, T. Gehoshi, and D. Ganser, J. Electron. Mater. 29, 376(2000).

Spe00 Spetz, A. L., P. Tobias, L. Unéus, H. Svenningstorp, L.-G. Ekedahl and I. Lundström, Sens. Actuators B70, 67(2000).

Spe97 Spetz, A. L., A. Baranzahi, P. Tobias, and I. Lundström, Phys. Stat. Sol. A162, 493(1997).

Ste76 Steele, M. C., J. W. Itile and B. A. MacIver, J. Appl. Phys. 47, 2537(1976).

Sti75 Stiblert, L. and C. Svensson, Rev. Sci. Instrum. 46, 1206(1975).

Sve99 Svenningstorp, H., P. Tobias, I. Lundström, P. Salomonsson, P. Mårtensson, L.-G. Ekedahl and A. L. Spetz, B57, 159(1999).

Sze81 Sze, S. M., Physics of Semiconductor devices, Wiley, New York(1981).

Tar01a Tarakji, A., G. Simin, N. Ilinskaya, X. Hu, A. Kumar, A. Koudymov, J. Yang, M. Asif Khan, M S. Shur, and R. Gaska, Appl. Phys. Lett. 78, 2169(2001)

Tar01b Tarplee, M. C., V. P. Madangarli, Z. Quinchun, T. S. Sudarshan, IEEE Trans. Electron. Dev. 48, 2659(2001).

Tar02 Tarakji, A., X. Hu, A. Koudynov, G. Simin, J Yang, M. A. Khan, M. S. Shur and R. Gaska, Solid-state electronics(in press).

Ter62 Terman, L. M., Solid-State Electron. 5, 285(1962).

The00 Therrien, R., G. Lucovsky, and R. F. Davis, Phys. Stat. Solidi A 176, 793(2000).

Tob97 Tobias, P., A. Baranzahi, A. L. Spetz, O. Kordina, E. Janzen and I. Lundstrom, IEEE Electron. Dev. Lett. 18, 287(1997).

Tri99 Trivedi, M. and K. Shenai, J. Appl. Phys. 85, 6889(1999).

Vas98 Vasiliev, A., W. Moritz, V. Fillipov, L. Bartholomäus, A. Terentjev and T. Gabusjan, Sens. Actuators B49, 133(1998).

Wal92 Waldrop, J. R., R. W. Grant, Y. C. Wang, and R. F. Davis, J. Applied Phys. 72, 4757(1992).

Wu97 Wu, Y.-F., B. P. Keller, S. Keller, D. Kapolnek, P. Kozodoy, S. P. DenBaars and U. K. Mishra, Solid-state Electron., 41, 1569(1997).

Zei00 Zeitouny, A., M. Eizenberg, S. J. Pearton, and F. Ren, J. Appl. Phys. 88, 2048(2000).

Zha00 Zhang, N.-Q., S. Keller, G. Parish, S. Heikman, S. P. DenBaars, and U. K. Mishra, IEEE Electron Device Lett. 21, 421(2000).

Zha03a Zhang, A. P., Materials Research Society, San Francisco (2003)

Zha03b Zhang, A. P., L. B. Rowland, E. B. Kaminsky, J. W. Kretchmer, R. A. Beaupre, J. L. Garrett, J. B. Tucker, B. J. Edward, J. Foppes and A. F. Allen, Sol.-State Electron. 47, 821(2003).

BIOGRAPHICAL SKETCH

Jihyun Kim was born in In-Cheon, South Korea, on August 27, 1974. He received his B.S. degree from Seoul National University in 2000. Also, he served in the Army for 26 months. He entered Ph.D. program in University of Florida, and joined Professor Fan Ren's group in 2000. He published over 60 technical journal papers, and was awarded the International Academic Award, Korean Graduate Student Research Award, and GRACE Symposium Award.

He did his internship with Dr. Hock Min Ng at Bell Laboratories during the winter of 2003.

His Ph.D. research topics include GaN gate-controlled diodes, wide bandgap gas senors, high temperature stable Schottky contacts, GaN-based enhancement-mode MOSFETs, GaMnN spintronics, high power devices, and irradiation hardness of wide bandgap semiconductor.

FOR THE COLLEGE OF ENGINEEERING

I certify that I have read this study and that in my opinion it conforms to acceptable standards of scholarly presentation and is fully adequate, in scope and quality, as a dissertation for the degree of Doctor of Philosophy.

Fan Ren, Chairman
Professor of Chemical Engineering

I certify that I have read this study and that in my opinion it conforms to acceptable standards of scholarly presentation and is fully adequate, in scope and quality, as a dissertation for the degree of Doctor of Philosophy.

Cammy R. Abernathy
Professor of Materials Science and Engineering

I certify that I have read this study and that in my opinion it conforms to acceptable standards of scholarly presentation and is fully adequate, in scope and quality, as a dissertation for the degree of Doctor of Philosophy.

Timothy J. Anderson
Professor of Chemical Engineering

I certify that I have read this study and that in my opinion it conforms to acceptable standards of scholarly presentation and is fully adequate, in scope and quality, as a dissertation for the degree of Doctor of Philosophy.

Stephen J. Pearton
Distinguished Professor of Materials Science and Engineering

This dissertation was submitted to the Graduate Faculty of the College of Engineering and to the Graduate School and was accepted as partial fulfillment of the requirements for the degree of Doctor of Philosophy.

May 2004

Pramod P. Khargonekar
Dean, College of Engineering

Winfred M. Phillips
Dean, Graduate School